Modelling and Analysing Orientation Fields of Fingerprints

Dissertation

zur Erlangung des Doktorgrades
der Mathematisch-Naturwissenschaftlichen Fakultäten
der Georg-August-Universität zu Göttingen

vorgelegt von

Thomas Hotz
aus Bruchsal

Göttingen 2007

D7

Referent:	Prof. Dr. Axel Munk
Koreferent:	Prof. Dr. Preda Mihăilescu
Tag der mündlichen Prüfung:	10. Juli 2007

Contents

Chapter 1

Introduction

1.1. Global features of fingerprints

In fingerprint analysis one distinguishes between *global* and *local* features which are used to describe and identify fingerprints: examples for local features are bifurcations and endings of fingerprint ridges (so-called *minutiae*) or sweat pores; the most widely used global features are *singular points* and the *orientation field* of a fingerprint. Throughout this thesis we will only be concerned with these global features; see e.g. (Maltoni et al. 2003) for a broad overview over the subjects of fingerprint analysis.

Intuitively, the *orientation field* at a point of a fingerprint pattern is given by the orientation parallel to the fingerprint ridges at this point, see Figure 1.1. Note that it is not a *directional* field as the ridges themselves are not oriented. Clearly, the orientation field is a global feature of the fingerprint as it is only well-defined on a scale large enough to give sense to the notion "parallel to the ridges". We will give a mathematical definition of an orientation field in Section 2.1.

As is visible from Figure 1.1, orientation fields may have *singular points*, i.e. points at which no orientation can be defined: discontinuities of the field. These singular points have been marked in Figure 1.1 as cores and deltas: a *core* is a point around which the ridges make at least a half-turn, a *delta* is a point where three ridges meet. This will also be formalised in Section 2.1: we will see that different singular points have different Poincaré indices.

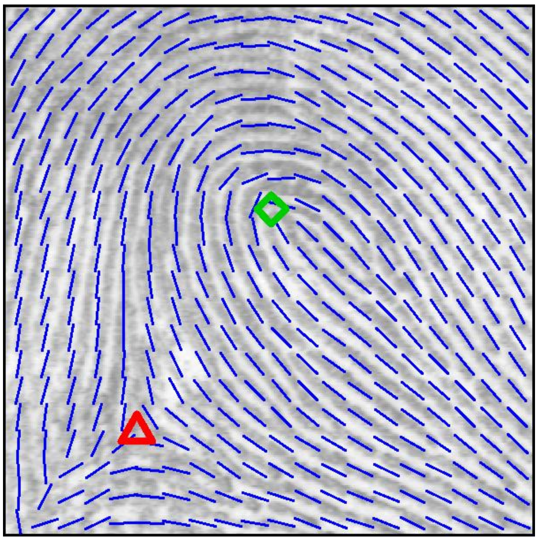

Figure 1.1. Orientation field and singular points of a fingerprint; ◊ marks a core, Δ a delta. Original image taken from (Watson and Wilson 1992).

Global features have been used in fingerprint analysis for a long time: Galton (1892) already used them to classify fingerprints into different classes though we adopt a slightly different and more modern terminology here, cf. Figure 1.2: an *arch* is a fingerprint featuring no singular point at all, *loops* and *tented arches* show one core and one delta, *whorls* and *twin-loops* have two deltas and one or two cores. Singular points thus capture the "topology" of a fingerprint, cf. (Penrose 1969) as well as (Sherlock and Monro

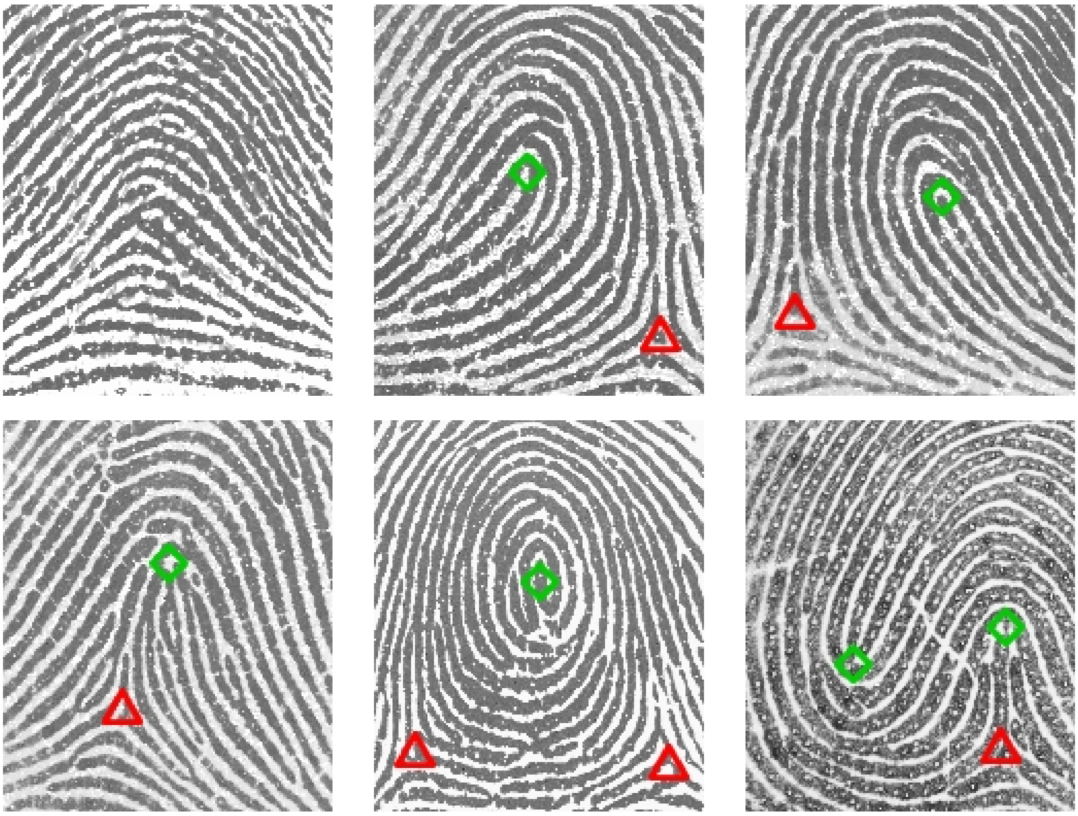

Figure 1.2. Fingerprint classes: arch, left loop, right loop (top); tented arch, whorl, twin-loop (bottom); △ marks a delta, ◊ a core. Note that there is an invisible delta further to the bottom left of the last image, which actually shows rather a tented-arch-and-loop than a twin-loop. Original images taken from (Maio et al. 2002).

1993). They allow, however, only for a very coarse description of a fingerprint. Indeed, classification schemes based on singular points allow only for few clearly distinguishable classes, cf. Bonnevie (1924) who conducted one of the first empirical studies on the distribution of these classes. Moreover, arches and tented arches occur only rarely in the population. The orientation field on the other hand contains additional information which might be used to describe fingerprints more precisely on a global scale. This is the reason why we are interested in its analysis.

Although they do not allow for discrimination between fingerprints of different fingers, there are several uses for global features in fingerprint analyses; we mention some of the more prominent ones:

(1) They are used for classifying fingerprints as well as for building continuous indices of them; both allow to reduce the search time for finding a matching fingerprint in a large database.

(2) Global features are also used when matching fingerprints: not only are the global features compared for a match but they are also used to aid the mapping of one fingerprint onto the other. Moreover, they are related to the distribution of the minutiae points.

(3) As global features can usually be extracted more robustly than local ones, they are often utilised for enhancing a fingerprint, e.g. by smoothing in the direction of the orientation field.

The aim to provide for these applications leads naturally to the quest for models of the orientation field. Before we come to that, we note some of the difficulties regularly encountered in fingerprint analyses:

Rotation and translation: imprints of the same finger vary since the finger will be rotated and translated differently each time an imprint is taken.

Partial observation: different imprints of the same finger show different regions, which, for instance, can mean that a singular point – usually a delta – is not observed in some imprint.

Non-linear distortion: varying amounts of pressure and possibly rotation when pressing the finger on the sensor surface result in non-linear distortions.

Large variations in contrast: fingerprints of greasy, wet and dry fingers show widely differing levels of contrast which has to be provided for when processing them.

Noise: Fingerprints show a large variety of noise and distortions: measurement noise including reflections on the scanner surface, (temporary) cuts in the finger surface, as well as phantoms left on the sensor surface, amongst others.

The impact of these problems, however, is greatly reduced when using global features. Note that they also depend heavily on the sensor being used to obtain the fingerprint: for a *live* image, most high-quality scanners require the user to *touch* a surface (e.g. a glass prism) leading to distortions and phantoms. Cheaper scanners frequently used in mobile devices provide only a narrow strip (usually a silicon chip measuring the skin's capacity) over which the finger is *swept*; from the resulting overlap of the many strips the full image is then computed, resulting in (erratic) distortions. *Direct reading* refers to a technology where the finger is photographed by a digital camera from a short distance; although avoiding some distortions and phantoms by being *touchless* (while introducing non-linear distortions through the projection), the acquisition of uniformly sharp and high-contrast images is difficult. In the forensic sciences one often uses digitally *scanned ink-prints* of fingers which usually vary strongly in contrast due to differing heights of ridges, amounts of ink, or pressure; the possibility to *roll* the finger over the paper however allows to obtain a fingerprint in its entirety. See (Maltoni et al. 2003, Chapter 2) for a detailed discussion of the different fingerprint sensing technologies.

1.2. Modelling orientation fields

In order to facilitate the use of orientation fields as global features in fingerprint analysis, we need numerical descriptions of them. In spite of the problems mentioned above, like partial observation for example, parametric models for orientation fields seem to be most promising. They naturally offer their uses in a variety of applications:

Compression: a small number of model parameters allows for memory-efficient storage of orientation fields.

Indexing: continuous parameters which do not change much between imprints of the same finger can be used for indices in databases as described in Section 1.1.

Extrapolation: parametric models can be used to extrapolate orientation fields into low-quality regions to aid enhancement and matching there.

Intrinsic coordinate systems: parametric models invariant under Euclidean motions can be used to define coordinates invariant under such transformations which in turn can be used during the matching stage.

Let us review some of the literature on models for orientation fields of fingerprints: Smith (1979) was one of the first to model orientation fields using differential equations; his work was later refined by Mardia et al. (1992). These early works were driven by the quest for differential equations whose trajectories have the structure of fingerprint ridges. More recently, Kücken and Newell (2004) have presented physically-motivated differential equations explaining the formation of fingerprints. All these studies aimed at a qualitative explanation of fingerprint patterns and cannot easily be used for the quantitative purposes we are striving for.

Sherlock and Monro (1993) took a slightly different approach: they used the argument of a complex rational function whose zeros and poles match the singular points of the fingerprint to model the orientation field. To make this precise, we will identify orientations with values on the unit circle $\mathrm{S}^1 \subset \mathbf{C}$, i.e. the orientation corresponding to some measured angle α will be represented as $e^{2\alpha i}$ where we have doubled the angle since orientations are undirected. For simplicity of presentation in this introduction, we will restrict ourselves to models for loops with a core at $c \in \mathbf{C}$ and a delta at $d \in \mathbf{C}$. Then Sherlock and Monro (1993) propose to model the loop's orientation at a point $z \in \mathbf{C}$ by

$$\frac{Q_{\mathrm{SM}}(z)^{-1}}{|Q_{\mathrm{SM}}(z)^{-1}|} \tag{1.1}$$

where

$$Q_{\mathrm{SM}}(z) = \alpha \, \frac{z-d}{z-c} \tag{1.2}$$

for some constant $\alpha \in \mathrm{S}^1$; note that we use the reciprocal of $Q_{\mathrm{SM}}(z)$ to easily relate this model to a corresponding mathematical object: in the terminology of complex analysis, Sherlock and Monro (1993) used a quadratic differential, actually the simplest one honouring the singular points; this relationship has first been noted by Huckemann et al. (2006). We will see in Sections 2.1 and 2.2 that indeed a (simple) zero of Q_{SM} gives rise to a delta, and a pole to a core.

The model of Sherlock and Monro (1993) has provided the starting point not only for the present work but also for several other authors: extensions have been proposed by Vizcaya and Gerhardt (1996), Gu and Zhou (2004) as well as by Gu et al. (2004), all aiming to increase the accuracy of that very simple model. Before we set out to propose models for orientation fields and subsequently analyse them, we need to compile a catalogue of properties that we expect such models to possess, such that they are of use for the applications mentioned above:

Accuracy: clearly, the model should fit the observed orientation field as precisely as possible.

Invariance under Euclidean motions: for model parameters to be useable as database indices, they need to be invariant under rotations and translations.

Robustness against partial observation: model parameters should be effected as little as possible when observing different parts of the same finger.

Low dimension: the number of parameters translates linearly into the amount of memory needed to store each orientation field in a database; moreover, increasing the number of parameters will most likely decrease the reliability of estimates of single parameters. For both reasons we are looking for models with as few parameters as possible.

Predictive power: for enhancing bad quality regions of fingerprints, such models should be useable for interpolation and possibly even extrapolation of the orientation field.

Interpretability: parameters ideally should have a geometrical meaning, i.e. they should relate to visible properties of the image and serve to understand the features of the model.

Obviously, it is not possible to fulfil all those requirements simultaneously: fewer parameters mean less flexibility – low-dimensional models generally will be less accurate than high dimensional ones. One therefore has to balance the different goals: we will try to find models that capture the main features of orientation fields whilst being as simple as possible. This can only be achieved through careful modelling, taking into account the geometrical properties shared by all fingerprints. We will propose models based on quadratic differentials in Section 2.3 which are determined by 5 real parameters only. The main idea is to extend the complex rational function of Sherlock and Monro (1993) by introducing artificial singular points outside the fingerprint domain in such a way that they reflect the geometry of a finger, and by incorporating the Euclidean motion directly into the model.

Let us sketch how we develop such a model; details are given in Section 2.3. We note that Q_{SM} quite accurately models the singular points and the "central area" of the fingerprint close to them, cf. Figure 2.2. It however fails to capture the flow of the ridges from the lower-left towards the fingertip, around the "central area" and down to the lower-right, cf. Figure 1.1. An orientation field with such a property is provided by

$$Q_k(z) = \frac{1}{(z-1)^k (z+1)^k} \tag{1.3}$$

for even k, which features two poles of order k at 1 and -1, respectively. The corresponding orientations given by $Q_k(z)^{-1}/|Q_k(z)^{-1}|$ are horizontal along the real axis, and form arches from one pole to the other on the upper half-plane, see Figure 2.3 for illustrations. We thus obtain a reasonable model for the "outer" or "background" field where the real axis represents the horizontal ridge along the finger's joint. We then combine this with the model of Sherlock and Monro (1993), see Equation (1.2), to obtain a full model for the finger by multiplying the respective rational functions, i.e. we consider

$$Q_{\mathrm{SM}}(z)\, Q_k(z) \tag{1.4}$$

and assume that core and delta lie in the upper half-plane between the poles of order k, see Figure 2.4(a). The orientations along the real axis now are no longer horizontal; this can be fixed however by mirroring core and delta across the real axis, see Figure 2.4(b). Since the finger ridges are horizontal below the joint, we also set the orientations horizontal on the lower half-plane, see Figure 2.4(c). We finally adapt this model to a given fingerprint by allowing it to independently scale along the real and imaginary axes, and by providing for a rotation and a translation. This gives us two (real) scaling parameters and three (real) parameters describing the Euclidean motion; the positions of core and delta can be extracted from the given fingerprint and therefore do not constitute free parameters. If one views the allowances for scaling and Euclidean motions as essential for any reasonable model for fingerprint orientation fields, then our models use a *minimal* set of 5 (real) parameters.

This "geometric" approach is in sharp contrast to the existing extensions by Vizcaya and Gerhardt (1996), Gu and Zhou (2004) as well as Gu et al. (2004) which improve the accuracy while sacrificing our other goals, see Section 2.4 for a discussion. The approach using quadratic differentials, however, will serve to review these models within a general framework, and to better understand the structure of such orientation fields. One particularly is interested in the "topology" of orientation fields within the medical field of *dermatoglyphics* where the relationship between singular points and certain genetical conditions, e.g. trisomies, is studied. Here, one not only analyses the orientation field on a single finger's volar pad (as in fingerprint analysis) but on the entire palm. It is then possible to diagnose e.g. Trisomy 18 (Edward's disease) with the help of the observed pattern, in this case by observing an excess number of arches, see Verbov (1970) for an overview. The study of quadratic differentials will allow us to derive Penrose's famous formula (Penrose 1969) of the relationship between the number of loops and deltas on an entire palm which is used in dermatoglyphics to ensure that all singular points have been detected (a more difficult task on the entire palm than on a finger's volar pad):

$$\text{number of deltas} + 1 = \text{number of fingers} + \text{number of loops} \tag{1.5}$$

where a *loop* is a core around which the ridges exactly make a half-turn, cores around which they make a full-turn are called *whorls* and have to be counted as two loops for reasons becoming apparent later, see Section 2.2.

Proposing models with good theoretical properties is not sufficient to show that they can be applied in ways envisaged beforehand: they need to be tested on and applied to real data. For the models we are going to propose it turns out that the main difficulty when trying to fit them to observed orientation fields lies in the determination of the imprint's particular rotation. Hence, an important part of this study lay in the development of algorithms which achieve just that, see Sections 3.2 and 3.3. They all are based on the observation that the model for the "outer" or "background" field in Equation (1.3) is symmetric with respect to the imaginary axis, cf. Figure 2.3, and subsequently aim to recover this symmetry axis. Clearly, the main part of the fingerprint that we observe is its "central area" where the symmetry axis is "hidden" under the field generated by the singular points, see Figure 1.2. This problem can be solved however by "inverting" Equation (1.4), i.e. by considering the orientation field

$$\psi(z) = \frac{Q_{\mathrm{SM}}(z)}{|Q_{\mathrm{SM}}(z)|}\phi(z), \tag{1.6}$$

where ϕ is the orientation field extracted from the fingerprint image together with the locations of the core and delta, cf. Equation (1.2). One could say that we obtained the "background" field ψ by "lifting" the singular points from the observed orientation field ϕ. We can then look for the symmetry axis of ψ. The most promising algorithm we propose for that task simply searches for the optimal axis such that ψ and its mirrored self are as similar as possible, see Section 3.3.

Using the NIST Special Database 4 (Watson and Wilson 1992) comprising 4000 fingerprint images – 2 imprints for each of 2000 fingers – we compared the usefulness of our newly proposed models with that of some existing models, namely the one by Sherlock and Monro (1993) as well as the one by Zhou and Gu (2004), see Chapter 4. To the best of our knowledge we are first to report such a large scale study for orientation field models. The results of this empirical study show that our proposed models were more accurate than the other two, by a considerable margin, see Section 4.1. Similarly, they gave better predictions than the others when we randomly cut out regions of the fingerprint and compared to the "ground truth", see Section 4.2. Also, the extracted parameters turned out to be rather stable between different imprints of the same finger, such that they could in principle be used for indexing, see Section 4.3. We finally used the algorithms for finding the symmetry axis and the models we proposed to define intrinsic coordinates, and analysed their stability. Although the vertical axes found were quite stable between different imprints of the same finger, the position of the horizontal axis proved more variable. Hence the symmetry axis found allows to define relatively precise intrinsic x-coordinates but the y-coordinates defined through the position of a model's horizontal axis are not very reliable, see Section 4.4.

Our empirical results now allow us to examine how well we have succeeded in reaching our aims, and how applicable these models really are. Indeed, our "geometric" approach proved successful in leading to simple, low-dimensional models whose parameters have a clear interpretation. They empirically appeared to be reasonably robust against partial observation, Euclidean motions etc. and showed their potential usability for a variety of applications. When compared to some models from the literature they were found to clearly outperform those. A more detailed discussion of their applicability, and on possible directions of further research has been provided in Chapter 5.

1.3. Outline

The organisation of the material presented is as follows: Chapter 2 introduces quadratic differentials and shows how they can be used to model orientation fields of fingerprints. In passing, we derive Penrose's formula and review some existing models from the literature within the framework of quadratic differentials. We will discuss implementation details for those models in Chapter 3. As mentioned above, a major difficulty lies in the extraction of a "symmetry axis" from the orientation field for which we will present two approaches in Sections 3.2 and 3.3. As we have different potential applications in mind for such models, we conducted a large study of different models using 4000 images, the results of which are to be found in Chapter 4. We conclude with a discussion in Chapter 5.

We record that, with the exception of Figure 1.1, all fingerprints shown and used to obtain the orientation fields visualised in the various figures throughout this text have been taken from the NIST Special Database 4 (Watson and Wilson 1992). Figure 2.1 was included by courtesy of Stephan Huckemann.

1.4. Acknowledgements

First and foremost I would like to thank my supervisor Axel Munk for giving me the opportunity to carry out this research. His continued trust in me finding and answering the right questions was very inspiring and drove me throughout the last three years. He always made it possible to find time to meet and talk about the research's progress. Also, I am much obliged to Preda Mihăilescu for his many thoughtful and thought-provoking comments on this work, regularly putting its applicability and usefulness to scrutiny, and thus ensuring its practical worth. To Stephan Huckemann I am deeply indebted for he not only initiated this research project and introduced me to the realms of quadratic differentials but in countless meetings provided a cooperative atmosphere in which we discussed results, envisioned new directions of research, and overcame a many obstacles. Additionally, he went to the trouble of carefully proof-reading this thesis from which it benefitted greatly. Furthermore, I thank Krzysztof Mieloch for his continuing support, especially for providing me with segmented versions of the database's images – not to mention his seemingly unlimited technical support. Moreover, I am most grateful to the Deutsche Forschungsgemeinschaft, Graduiertenkolleg 1023 "Identifikation in mathematischen Modellen: Synergie stochastischer und numerischer Methoden", for its financial support and the enjoyable, stimulating environment it provided – thanks to all its members, particularly my office-mate Carsten Gottschlich. Similarly, my colleagues at the Institute for Mathematical Stochastics always encouraged me by making it a pleasure to come to Göttingen.

Last but certainly not least I express my deepest gratitude to my wife Sonja – during these years she gave me to eat and drink, a place to sleep, trying everything to motivate me even when I was the least interested in working at all. She pushed me when I needed it and cared for me when I struggled – and then she also proof-read the entire manuscript! Without her, this thesis would never have been finished.

Chapter 2

Models for Orientation Fields

This chapter starts out with a formal definition of orientation fields and singular points, our main objects of interest. Their relationship to quadratic differentials will become apparent in Section 2.2 where we cite some results from complex analysis which will allow us to model orientation fields by quadratic differentials as demonstrated in Section 2.3. Finally, we review some models from the literature within this framework, see Section 2.4.

2.1. Orientation fields and singular points

Although we observe our data only on a finite grid, we will model the area of a fingerprint as a domain $D \subseteq \hat{\mathbf{C}}$ where $\hat{\mathbf{C}} = \mathbf{C} \cup \{\infty\}$. The reason for considering the whole Riemann sphere will become clear later: the study of orientation fields greatly benefits when they are considered on a compact manifold, see Remark 2.14; note also that Sherlock and Monro (1993) already gave their free parameter the meaning of an orientation at ∞, cf. Definition 2.6 and Equation (2.10). Since an orientation given as an angle α is uniquely determined only modulo π, we identify it with $(e^{i\alpha})^2 = e^{i2\alpha}$ which is equivalent to doubling the angle. Hence, orientations are uniquely represented by their values on the unit circle $\mathrm{S}^1 = \{z \in \mathbf{C} : |z| = 1\}$. We are now in a position to give a mathematical definition of our main object of interest:

Definition 2.1. *A* meromorphic orientation field *on a domain $D \subseteq \hat{\mathbf{C}}$ is a mapping $\phi : D \setminus N \to \mathrm{S}^1$ which has a meromorphic representation $f : D \to \hat{\mathbf{C}}$ with $\phi(\cdot) \equiv \frac{|f(\cdot)|}{f(\cdot)}$ where $N = \{z \in D \mid f(z) = 0 \vee f(z) = \infty\}$ is the set of* singular points *of ϕ.*

Later, when we introduce quadratic differentials in Section 2.2, it will become apparent why we are using the reciprocal of f.

In general, an *orientation field* (with isolated singular points) will be a diffeomorphic[1] deformation of a meromorphic orientation field; as the only non-conformal transformations we are going to consider are ($\mathbf{R}^2$-) linear transformations, we will not formalise this notion, cf. Definition 2.6 and Remark 2.7.

Definition 2.2. *A* simple zero *of the meromorphic representation f of an orientation field ϕ is called a* delta *of ϕ, a* pole *of f is called a* core *of ϕ; any zero or pole of f is called a*

[1] Note that we call a mapping from $\mathbf{C}$ to $\mathbf{C}$ *diffeomorphic* if it is a C^1-diffeomorphism between real vector spaces, i.e. when we identify $\mathbf{C}$ with $\mathbf{R}^2$. If the mapping additionally is ($\mathbf{C}$-) analytic we call it *conformal*.

singular point *of ϕ. We say ϕ is of* order k *at z if k is the order of f at z_0 in its Laurent power series expansion, i.e. zeros have positive order, poles have negative order and ordinary points have order* 0*. The* order *of ϕ on D is the sum of the orders of ϕ at all points $z \in D$ if there are only finitely many z with non-zero order.*

As fingerprints do not feature zeros of higher orders, we do not concern ourselves with them here.

In the engineerings literature, singular points are usually defined through their Poincaré index:

Definition 2.3. *For a point z_0 in D, the domain of a meromorphic orientation field ϕ, let $r > 0$ be such that the closed unit disc with centre z_0 and radius r is contained in D and does not contain any singular points of ϕ except possibly z_0. Further let $\alpha : [0, 2\pi] \to \mathbf{C}$ with $\alpha(t) = z_0 + re^{it}$. Then the Poincaré index of ϕ at z_0 is defined as*

$$\frac{1}{4\pi}\int_0^{2\pi}\left(\frac{d}{dt}\arg(\phi(\alpha(t)))\right)dt. \tag{2.1}$$

Note that we use 4π instead of 2π in the denominator since we have doubled the angles. It is easy to see that the Poincaré index at a point is well-defined, invariant under diffeomorphic transformations, and equals zero for a non-singular point of ϕ in view of α being null-homotopic in that case. One immediately gets the following

Lemma 2.4. *With the notation of Definition 2.3 the Poincaré index of ϕ at the point z_0 equals $-\frac{k}{2}$ where k is the order of ϕ at z_0.*

Thus a point is a delta iff its Poincaré index is $-\frac{1}{2}$, it is a core iff its index is positive, leading to an equivalent definition of singular points which is frequently used in the fingerprint analysis literature, see e.g. Sherlock and Monro (1993).

2.2. Quadratic differentials

We are now going to introduce quadratic differentials, citing and motivating some of their properties, see e.g. Jensen (1975) for an introduction, or Strebel (1984) for a more thorough treatment of the subject.

In the following we will identify line elements dz with elements in $\mathbf{C}^* = \mathbf{C} \setminus \{0\}$.[2] One way to interpret dz is as the (non-zero) velocity of a curve through z, cf. the remarks on trajectories below. Note that squaring[3] and normalising a line element dz gives the orientation of that line element, $\frac{dz^2}{|dz^2|}$.

Definition 2.5. *A* quadratic differential *on a domain $D \subseteq \hat{\mathbf{C}}$ is a mapping $\sigma : D \times \mathbf{C}^* \to \hat{\mathbf{C}}$ which can be represented as $\sigma(z, dz) = Q(z)\ dz^2$ where $Q : \hat{\mathbf{C}} \to \hat{\mathbf{C}}$ is meromorphic.*[4]

The quadratic differential σ determines a meromorphic orientation field by imposing the condition

$$\sigma(z, dz) = Q(z)\ dz^2 > 0 \tag{2.2}$$

[2]Formally, a line element is a non-zero tangent vector at a point z of a Riemannian manifold. Since we are only considering subsets of $\hat{\mathbf{C}}$, we choose the identical chart on $\mathbf{C}$ and canonically identify the tangent space with $\mathbf{C}$ itself; at ∞ we will use the chart $z \mapsto z^{-1}$ if needed.

[3]Here and elswhere, dz^2 is shorthand for $(dz)^2$; d by itself bears no meaning.

[4]The representation of σ via Q at ∞ will be defined via the transformation rule in Definition 2.6 under the map $z \mapsto z^{-1}$, cf. Footnote (2).

on the line elements, i.e. there is a uniquely determined orientation field ϕ on D such that $Q(z)\ \phi(z) > 0$. A simple calculation shows that ϕ is represented by Q, i.e. $\phi(z) = \frac{|Q(z)|}{Q(z)}$, cf. Definition 2.1.

A curve $\gamma : (a, b) \to D$ is called a *trajectory* of σ if its tangent vectors[5] fulfil the condition in Equation (2.2), i.e. if $Q(\gamma(t))\ \dot{\gamma}(t)^2 > 0$ for all $t \in (a, b)$. We obtain a trajectory through a non-singular point[6] z of σ by solving the differential equation

$$\dot{\gamma}(t) = \sqrt{\frac{1}{Q(\gamma(t))}} \tag{2.3}$$

with initial condition[7] $\gamma(0) = z$. Note that for any non-singular point there is always a trajectory through it.

We will make use of the following transformation rule for quadratic differentials:

Definition 2.6. *Let $f : D \to f(D) \subseteq \hat{\mathbf{C}},\ z \mapsto w = f(z)$ be a conformal mapping, $\sigma(z, dz) = Q(z)\ dz^2$ a quadratic differential on D. Then $\tau : f(D) \times \mathbf{C}^* \to \mathbf{C}$ is the* transformed *quadratic differential if $\tau(w, dw) = P(w)\ dw^2 = Q(z)\ dz^2 = \sigma(z, dz)$. Here, $dw = f'(z)\ dz$ denotes the transformed line element.*

Clearly, the transformed quadratic differential is given by

$$P(w)\ dw^2 = \frac{(Q \circ f^{-1})(w)}{\big((f' \circ f^{-1})(w)\big)^2}\ dw^2 \tag{2.4}$$

for all $w \in f(D)$.

Remark 2.7. One easily derives a similar transformation rule for a non-conformal, diffeomorphic f.

The following simple corollary to Definition 2.6 justifies our way of transforming quadratic differentials, cf. also Theorem 2.12:

Lemma 2.8. *Under the assumptions of Definition 2.6, P is meromorphic whenever Q is, the order of σ at $z \in D$ equals the order of τ at $f(z)$, and trajectories of σ are mapped onto trajectories of τ.*

An important consequence of the transformation rule describes the global behaviour of quadratic differentials on the Riemann sphere:

Corollary 2.9. *The order of any quadratic differential σ on $\hat{\mathbf{C}}$ is -4.*

We emphasise that only classical complex analysis is needed to obtain the results quoted here; to give a flavour of the arguments used we present a short proof of the above corollary:

Proof. Let $\sigma(z, dz) = Q(z)\ dz^2$. Since Q is meromorphic on $\hat{\mathbf{C}}$, Q is a rational function, i.e. there are points $c_1, \ldots, c_m, d_1, \ldots, d_n \in \mathbf{C}$ with $c_i \neq d_j$ for $i = 1, \ldots, m$ and $j = 1, \ldots, n$ such that

$$Q(z) = \frac{\prod_{j=1}^{n}(z - d_j)}{\prod_{i=1}^{m}(z - c_i)}. \tag{2.5}$$

[5] We denote differentiation with respect to the parameter of the curve γ by a dot, $\dot{\gamma}(t) = \frac{d}{dt}\gamma(t)$.

[6] Notions defined for orientation fields can also be transferred to quadratic differentials by applying them to the corresponding orientation field.

[7] Here, we can choose either branch of the square-root; choosing the other one only reverses the direction.

We now consider the transformation $f(z) = z^{-1}$ which will allow us to compute the order of σ at ∞. According to Equation (2.4) the transformed quadratic differential $P(w)\ dw^2$ is given by

$$P(w) = \frac{Q(w^{-1})}{\big(-(w^{-1})^{-2}\big)^2} = -w^{-4}\frac{\prod_{j=1}^n (w^{-1} - d_j)}{\prod_{i=1}^m (w^{-1} - c_i)} = -w^{-4-n+m}\frac{\prod_{j=1}^n (1 - d_j w)}{\prod_{i=1}^m (1 - c_i w)}. \tag{2.6}$$

Thus the order of P at 0 in its Laurent power series expansion is $-4 - n + m$, which equals the order of σ at ∞. Thus the order of σ is $n - m - 4 - n + m = -4$. □

Remark 2.10. It is possible to extend this analysis to arbitrary compact Riemann surfaces, the order of a quadratic differential d is then an invariant related to the topological genus g of the surface, namely $d = 4g - 4$; this is a consequence of the Riemann-Roch theorem, cf. (Farkas and Kra 1980, Corollary 2, p. 74).

The main result about quadratic differentials that we are going to need describes the local structure of their trajectories, see e.g. (Jensen 1975, Theorem 8.2); observe from Definition 2.6 that it is sufficient to consider subdomains of $\mathbf{C}$ when studying a quadratic differential locally since the behaviour at ∞ can be inferred using a suitable chart.

Theorem 2.11. *Consider a quadratic differential $\sigma(z, dz) = Q(z)\ dz^2$ on a domain $D \subseteq \mathbf{C}$. If $z \in D$ is*

- *an ordinary point, i.e. Q has a Laurent power series expansion of order 0 at z, then there is exactly one trajectory through z, see Figure 2.1(a);*
- *a zero of order k, then there are exactly $k + 2$ trajectories emanating from z at regularly distributed angles, see Figure 2.1(b);*
- *a pole of order 1, then there is exactly one trajectory ending at z, see Figure 2.1(c);*
- *a pole of order 2, then the structure in a sufficiently small neighbourhood U further depends on the lowest order coefficient in the expansion, $a_{-2} = \lim_{\zeta\to z}\zeta^2 Q(\zeta)$:*
  - *if $a_{-2} < 0$ no trajectory ends at z and any trajectory through $\zeta \in U$, $\zeta \neq z$ is closed, see Figure 2.1(d);*
  - *if $a_{-2} > 0$ any trajectory through $\zeta \in U$, $\zeta \neq z$ ends at z and no two distinct trajectories ending at z have the same limiting direction there, see Figure 2.1(e);*
  - *for any other $a_{-2} \notin \mathbf{R}$ any trajectory through $\zeta \in U$, $\zeta \neq z$ has z as a limit point, spiralling around it infinitely often, see Figure 2.1(f);*
- *a pole of order $k > 2$, then there is a neighbourhood U of z such that any $\zeta \in U$, $\zeta \neq z$ is connected with z by a trajectory and all such trajectories meet at z at k regularly distributed limiting directions, see Figure 2.1(g)-(h).*

This theorem is proven by direct calculation starting from the so-called *Normal-Form Theorem* (Jensen 1975, Theorem 8.1):

Theorem 2.12. *Let $\sigma(z, dz) = Q(z)\ dz^2$ be a quadratic differential on a domain $D \subseteq \hat{\mathbf{C}}$. Then for any $z_0 \in D$ there is a neighbourhood U of z_0 and a conformal mapping $z \mapsto w = f(z)$ such that the transformed quadratic differential fulfils*

$$Q(z)dz^2 = \begin{cases} dw^2 & \text{if } z_0 \text{ is an ordinary point,} \\ w^k\ dw^2 & \text{if } z_0 \text{ is a zero of order } k, \\ w^{-k}\ dw^2 & \text{if } z_0 \text{ is a pole of odd order } k, \\ a_{-2}w^{-2}\ dw^2 & \text{if } z_0 \text{ is a pole of order } 2, \\ (w^{-k/2} + \sqrt{a_{-2}}w^{-1})^2\ dw^2 & \text{if } z_0 \text{ is a zero of odd order } k \geq 4, \end{cases} \tag{2.7}$$

where a_{-2} is defined as in Theorem 2.11.

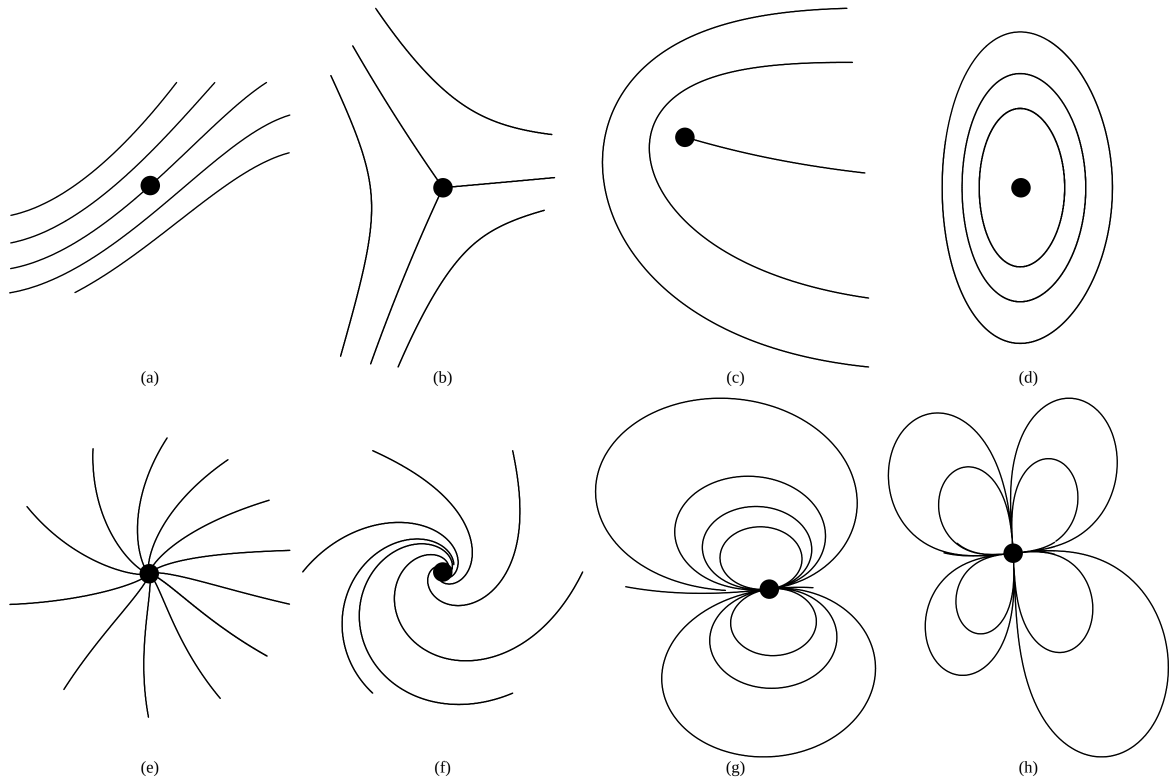

Figure 2.1. Behaviour of trajectories near points of different orders, see Theorem 2.11: (a) ordinary point, (b) simple zero, (c) simple pole, (d) double pole with $a_{-2} < 0$, (e) double pole with $a_{-2} > 0$, (f) double pole with $a_{-2} \notin \mathbf{R}$, (g) fourth-order pole, (h) sixth-order pole. Illustration courtesy of Stephan Huckemann.

One proves this theorem using Equation (2.4) while carefully distinguishing the cases of poles of order 2, higher odd order poles, and points of any other order. Note that a_{-2} plays a special rôle for poles of odd orders since $\sqrt{a_{-2}}$ is the residue of $\sqrt{Q}$.

We conclude this section noting some of the areas in which quadratic differentials are used:

Remark 2.13. Historically, quadratic differentials have been introduced by Grötzsch (1929) and Teichmüller (1940) during the 1930s in their studies of invariants of Riemann surfaces, citing only two of their many works on the subject. Subsequently, quadratic differentials played a fundamental rôle in the development of Teichmüller theory due to their close relationship to extremal quasiconformal mappings and Teichmüller maps, cf. e.g. (Gardiner 1987). More recently, they have been used to study the ergodicity of dynamical systems (Kerckhoff et al. 1986) as well as defects and textures of crystals (Kholodenko 2000), to give just two examples showing their current use in a broad range of applications.

2.3. Models based on quadratic differentials

Comparing the trajectories of quadratic differentials in Figure 2.1 with the ridge structure of fingerprints in Figure 1.2, one immediately understands how they relate to orientation fields of fingerprints: reasonable models for them are given by quadratic differentials whose zeros and poles match the deltas and cores of the fingerprint according to Definition 2.2. This connection between orientation fields of fingerprints and quadratic differentials has been noted by Stephan Huckemann and initiated the present work, cf. (Huckemann, Hotz and Munk 2006).

Let us from now on assume that D is the area of the fingerprint which we observe, containing *all* singular points of the fingerprint. Empirically, one observes that there are at most two deltas and two cores in a fingerprint.

Remark 2.14. The orientation field of a fingerprint has empirically found to have order 0. This is to be expected from Corollary 2.9: a fingertip can be viewed as topologically being equivalent to a half-sphere, where the ridges flow along the joint, i.e. along the equator. We thus can continue the field onto the Riemann sphere if we place a second-order pole on the other half-sphere. Further note that fingerprint ridges flow along the border of the fingernail, which henceforth also can be represented as a second-order pole. These are the only "boundary conditions". From Corollary 2.9 we know that the order on the Riemann sphere is -4, and the boundary conditions already account for an order of -4, leaving order 0 for the orientation field of the fingerprint itself. (One could also identify the boundary of the fingernail with the joint, obtain a torus and use the fact that the order of a quadratic differential on a torus is 0, cf. Remark 2.10.)

Similar arguments allow us to derive Penrose's formula (Penrose 1969) about the number of loops and deltas on an entire palm:

$$\text{number of deltas} + 1 = \text{number of fingers} + \text{number of loops}, \tag{2.8}$$

where a whorl counts as two loops. Since the number of deltas equals the number of zeros of the corresponding quadratic differential on the palm and the number of loops then equals the number of poles counting multiplicities, this formula is equivalent to asserting that the order of a quadratic differential on the entire palm is one less than the number of fingers. Let us now derive this property of orientation fields on the entire palm: like before, we consider the entire hand as a half-sphere with ridges parallel to the wrist represented as the equator. Thus on the entire hand the order of the orientation field must be -2 due to the "boundary condition" on the equator. We now argue by induction, starting with a hand with one finger: since the finger has again one fingernail being equivalent to a second-order pole, indeed the order of the orientation field is 0, one less than the number of fingers. If we now add a finger, we add an order of -2 due to the finger's "boundary condition" as above; at the same time we will have to add two deltas – one on the palm and one on the back of the hand, i.e. the order of the orientation field on the palm increases by one, which proves the induction step and thus Penrose's formula.

The above deliberations lead one to consider the following rational function which has first been proposed by Sherlock and Monro (1993), albeit without a rigorous justification:

$$Q_{c_1,c_2,d_1,d_2}(z) = \frac{(z-d_1)(z-d_2)}{(z-c_1)(z-c_2)} \ , \tag{2.9}$$

where c_1 and c_2 are the locations of (simple) cores, d_1 and d_2 are the locations of deltas; for a whorl we set $c_1 = c_2$ resulting in a second-order pole; for a loop or tented arch set $c_2 = d_2$ arbitrary leaving only one core and one delta; and for an arch set $c_1 = d_1 = c_2 = d_2$ arbitrary such that all terms cancel, leaving no singular point at all. Thus Q_{c_1,c_2,d_1,d_2} incorporates all possible singular points in a fingerprint.

To account for rotations of the finger, Sherlock and Monro (1993) suggest to use the following quadratic differential for modelling the orientation field of a fingerprint:

$$\sigma_{\mathrm{SM}}(z,dz) = \alpha\, Q_{c_1,c_2,d_1,d_2}(z)\, dz^2, \tag{2.10}$$

where $\alpha \in \mathbf{C}$ gives the orientation at ∞. This model is far too simplistic: for an arch it results in parallel trajectories whose orientations are $|\alpha|/\alpha$ – thus modelling the *arches* not at all, see Figure 2.2. Observe however that the model improves as the number of singular

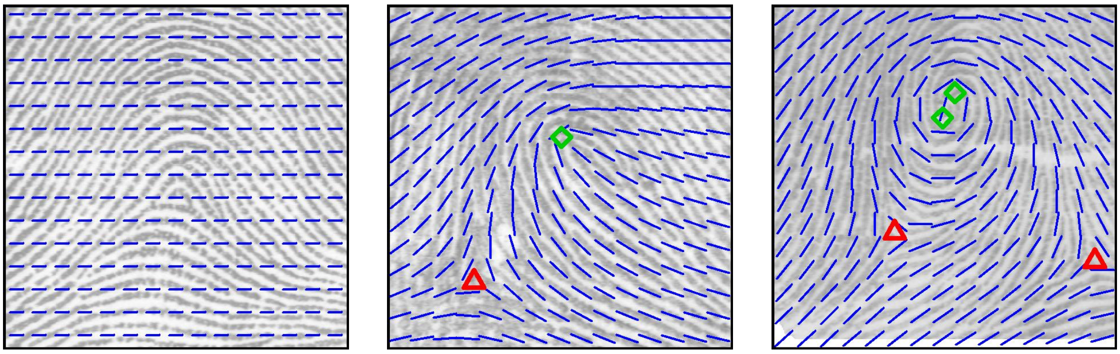

Figure 2.2. Model σ_{SM} of Sherlock and Monro (1993) fitted to the orientation fields of an arch, a right loop and a whorl, respectively.

points increases: this is to be expected since the field in the centre of the fingerprint is then dominated by these singular points which can adequately be modeled by Q_{c_1,c_2,d_1,d_2}.

Before proposing improvements for this model, we note that Q_{c_1,c_2,d_1,d_2} will only model the ridge structure in the central part of the fingerprint; its effects vanish if we move away from the singular points. More precisely:

Lemma 2.15. *Assume we have two singular points, a core at $c \in \mathbf{C}$ and a delta at $d \in \mathbf{C}$, i.e. we are interested in the behaviour of the quadratic differential $Q(z)\ dz^2$ given by $Q(z) = \frac{z-d}{z-c}$. Then the orientation field $\phi(z) = \frac{|Q(z)|}{Q(z)}$ generated by this quadratic differential fulfils*

$$\tan\arg\phi(z) = \frac{\sin\alpha}{\frac{|z-d|}{|d-c|} + \cos\alpha}\ , \tag{2.11}$$

where $\alpha = \arg(z-d) - \arg(d-c)$ is the angle between the line connecting z with the delta and the line connecting the delta with the core.[8]*.*

Proof. We start from

$$Q(z)^{-1} = \frac{z-c}{z-d} = \frac{z-d+d-c}{z-d} = 1 + \frac{d-c}{z-d} = 1 + P^{-1}, \tag{2.12}$$

where $P = \frac{z-d}{d-c}$ such that $\alpha = \arg P$. Then, using that for $w \in \mathbf{C}^*$

$$\sin\arg w = \frac{w-\bar{w}}{2i|w|}\ , \quad \cos\arg w = \frac{w+\bar{w}}{2|w|}\ , \quad \text{and} \quad \tan\arg w = i^{-1}\frac{w-\bar{w}}{w+\bar{w}}\ , \tag{2.13}$$

we have that

$$\begin{aligned} i\tan\arg\phi(z) &= i\tan\arg Q(z)^{-1} = \frac{Q(z)^{-1} - \overline{Q(z)^{-1}}}{Q(z)^{-1} + \overline{Q(z)^{-1}}} = \frac{P^{-1} - \overline{P^{-1}}}{2 + P^{-1} + \overline{P^{-1}}} \\ &= \frac{\bar{P} - P}{2|P|^2 + P + \bar{P}} = \frac{-i^{-1}\sin\arg P}{|P| + \cos\arg P} = i\frac{\sin\alpha}{\frac{|z-d|}{|d-c|} + \cos\alpha}\ . \end{aligned} \tag{2.14}$$

$\square$

Corollary 2.16. *Generalising the above result, let $Q(z) = \prod_{i=1}^n \frac{(z-d_i)^{k_i}}{(z-c_i)^{k_i}}$ for $k_i \in \mathbf{N}$, $i = 1, \ldots, n$, and let $\phi(z) = \frac{|Q(z)|}{Q(z)}$. Then*

$$\arctan|\arg(\phi(z))| \ \le\ \sum_{i=1}^n k_i \frac{\sin\alpha_i}{\frac{|z-d_i|}{|d_i-c_i|} + \cos\alpha_i}\ , \tag{2.15}$$

[8] Note that the left-hand side is infinite whenever the right hand side is; this happens iff z lies on the circle through c and d with centre $(c+d)/2$

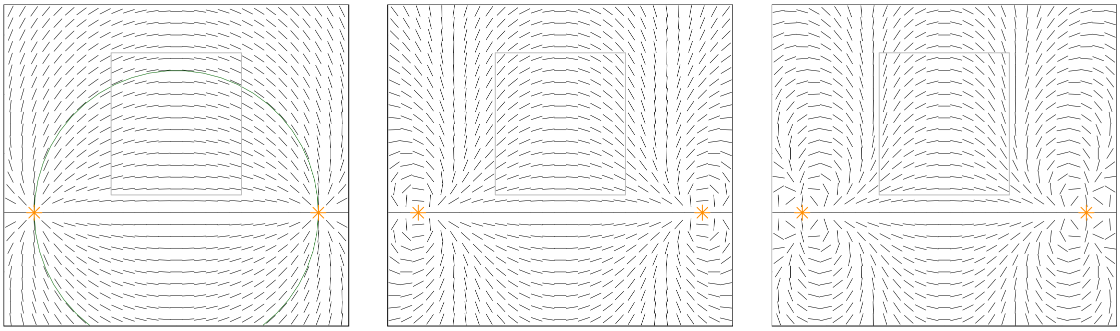

Figure 2.3. Orientation fields generated by σ_2, σ_4 and σ_6, respectively. The artificial poles have been marked by orange stars. The hypothetical fingerprint area is shown as a grey window. The green unit circle is a trajectory of σ_2.

where $\alpha_i = |\arg(z - d_i) - \arg(d_i - c_i)|$. *In particular,*

$$|\arg(\phi(z))| \;\le\; \sum_{i=1}^{n} k_i \min\left\{ \sin\alpha_i \frac{|d_i - c_i|}{|z - d_i|},\, \tan\alpha_i \right\}. \tag{2.16}$$

Proof. This is immediate from Lemma 2.15; note that $\arctan\beta \le \beta$ for $\beta \in [0, \pi/2)$. □

Remark 2.17. Since $|\arg\phi(z)| = |\arg Q^{-1}(z)| = |\arg Q(z)|$, we can interchange the rôles of c_i and d_i for any i and thus the above results remain valid for $\alpha_i = |\arg(z - c_i) - \arg(c_i - d_i)|$ if we substitute $|z - d_i|$ by $|z - c_i|$.

Hence the influence of cancelling singular points declines as the reciprocal distance to them. Thus Q_{c_1,c_2,d_1,d_2} indeed will model only the central part of the fingerprint and we are left with the problem of adequately modelling the outer part of the finger, i.e. its global ridge structure.

We observe, cf. Figure 1.2, that the ridges are parallel to the joint of the second and third phalanx, i.e. they are horizontal at the bottom of a properly aligned fingerprint, and they are circular or elliptic near the finger tip, cf. Remark 2.14. We can most easily create a field with these properties by placing two artificial poles of identical order outside the observed fingerprint region at the line representing the joint. For now we will assume that the fingerprint is aligned such that the real axis represents the joint, and it is scaled such that $D \subset \{z \in \mathbf{C} \mid -1 < \operatorname{Re} z < 1\}$, i.e. the fingerprint region is contained in the vertical strip between -1 and 1. Then a simple model for the outer field of a fingerprint is given through

$$\sigma_k(z, dz^2) = \frac{1}{(z-1)^k (z+1)^k}\, dz^2 = \frac{dz^2}{(z^2-1)^k} \tag{2.17}$$

for even $k \in \mathbf{N}$. Note that the real line is a trajectory of σ_k as required. Furthermore, there is a trajectory through every purely imaginary z crossing the imaginary axis horizontally and connecting z with both poles. This results in the trajectories forming arches as required, see Figure 2.3.

Starting from this outer – or background – field, we add the singular points by multiplication with $Q_{c_1,c_2,d_1,d_2}(z)$, i.e. we consider

$$Q_{c_1,c_2,d_1,d_2}(z)\; \sigma_k(z, dz). \tag{2.18}$$

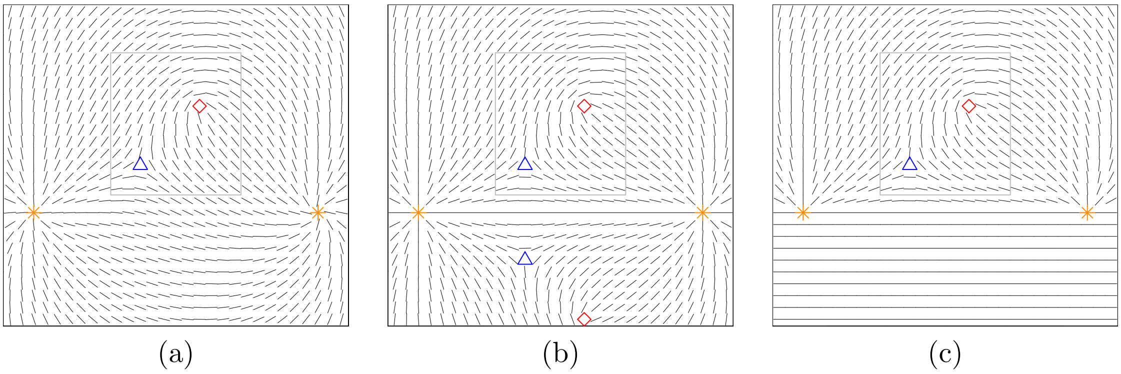

Figure 2.4. Construction of $\sigma_{\text{basic},k}$: orientation fields for a loop generated by the quadratic differentials of Equations (2.18) to (2.20), respectively, for $k = 2$.

Now, the real line no longer is a trajectory any more, see Figure 2.4(a). To fix this, we restore the symmetry with respect to the real axis by mirroring all singular points across it. We thus artificially add simple poles $\bar{c}_1$, $\bar{c}_2$ and zeros $\bar{d}_1$, $\bar{d}_2$, leading to the quadratic differential

$$Q_{c_1,c_2,d_1,d_2}(z)\ Q_{\bar{c}_1,\bar{c}_2,\bar{d}_1,\bar{d}_2}(z)\ \sigma_k(z, dz) = \frac{(z-d_1)(z-d_2)}{(z-c_1)(z-c_2)}\ \frac{(z-\bar{d}_1)(z-\bar{d}_2)}{(z-\bar{c}_1)(z-\bar{c}_2)}\ \frac{dz^2}{(z^2-1)^k}. \tag{2.19}$$

Figure 2.4(b) shows that indeed the real axis is a trajectory again, a fact easily verified. Noting that near to and beyond the joint of a fingerprint the ridges are parallel we extend the field from the upper half plane continuously to the lower half plane by parallel lines, see Figure 2.4(c):

$$\sigma_{\text{basic},k}(z, dz) = \begin{cases} Q_{c_1,c_2,d_1,d_2}(z)\ Q_{\bar{c}_1,\bar{c}_2,\bar{d}_1,\bar{d}_2}(z)\ \sigma_k(z, dz) & \text{for } \operatorname{Im} z > 0, \\ dz^2 & \text{for } \operatorname{Im} z \leq 0. \end{cases} \tag{2.20}$$

This is the *basic* model for the orientation field of a fingerprint. See Figure 2.4(c) and Figure 2.5(a)-(b) for an illustration of $\sigma_{\text{basic},k}$ with $k = 2, 4, 6$ for a right loop. Note that using poles of order $k \geq 8$ does not change the qualitative behaviour of the trajectories in the region we are considering, cf. also Figure 2.1, but that they have empirically been found to lead to instabilities if they get too close to the fingerprint domain. We thus consider only poles of order 2, 4 or 6.

Recalling that the ridges are circular or elliptic near the fingertip, we might want to incorporate this into our model as well. From Figure 2.3 we see that σ_2 has the unit circle

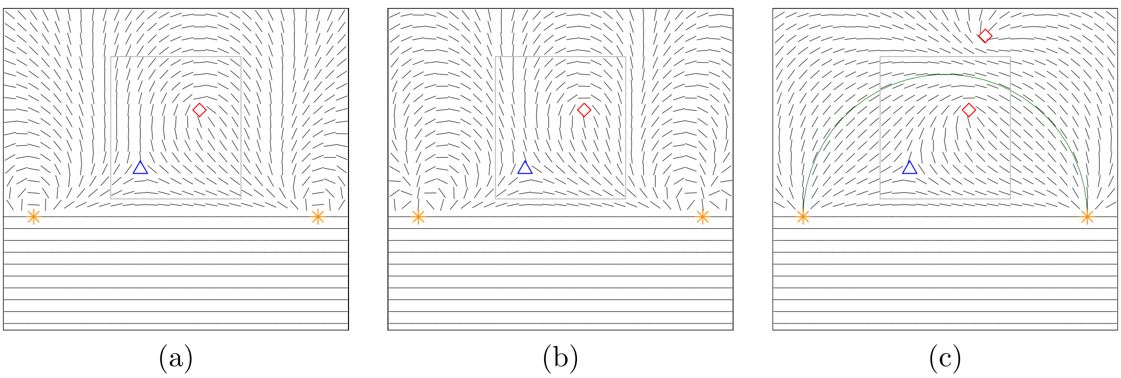

Figure 2.5. Orientation fields for a loop generated by the quadratic differentials of $\sigma_{\text{basic},4}$, $\sigma_{\text{basic},6}$, and σ_{circ}, respectively. The green upper half of the unit circle is a trajectory of σ_{circ}.

as a trajectory; after the introduction of the singular points this property is lost, however. We can restore it by additionally mirroring all singular points, including the artificial ones, across the unit circle, i.e. we add simple poles $1/c_1$, $1/c_2$, $1/\bar{c}_1$, $1/\bar{c}_2$ and zeros $1/d_1$, $1/d_2$, $1/\bar{d}_1$, $1/\bar{d}_2$. This results in the *circular* model

$$(2.21)\qquad \sigma_{\text{circ}}(z,dz) = \begin{cases} Q_{\frac{1}{c_1},\frac{1}{c_2},\frac{1}{d_1},\frac{1}{d_2}}(z)\ Q_{\frac{1}{\bar{c}_1},\frac{1}{\bar{c}_2},\frac{1}{\bar{d}_1},\frac{1}{\bar{d}_2}}(z)\ \sigma_{\text{basic},k}(z,dz) & \text{for } \operatorname{Im} z > 0, \\ dz^2 & \text{for } \operatorname{Im} z \leq 0. \end{cases}$$

It again possesses the real line and the upper half of the unit circle as trajectories, see Figure 2.5(c). Indeed, for $|z| = 1$, $\operatorname{Im} z > 0$, noting $z^{-1} = \bar{z}$,

$$(2.22)\qquad (z-a)(z-a^{-1})(z-\bar{a})(z-\bar{a}^{-1}) = z^2\ |a|^2\ (z-a)(a-\bar{z})(z-\bar{a})(\bar{a}-\bar{z}) = c_a(z)\ z^2$$

with $c_a(z) > 0$. We thus get for $dz = iz$ which is tangential to the unit circle, and for some $c(z) > 0$,

$$(2.23)\qquad \sigma_{\text{circ}}(z,dz) = c(z)\ \frac{dz^2}{(z^2-1)^2} = c(z)\ \frac{(iz)^2}{(2i \operatorname{Im} z)^2 z^2} > 0$$

as required.

Finally, we adapt these models ($\sigma_{\text{basic},k}$ and σ_{circ}) to a given fingerprint by allowing for the following $\mathbf{R}^2$-linear transformations: firstly, we rescale allowing different scaling parameters horizontally and vertically, i.e. we consider

$$(2.24)\qquad z' = S_{s_x,s_y}(z) = s_x \operatorname{Re} z + i\, s_y \operatorname{Im} z$$

for $s_x, s_y \in \mathbf{R}$. Note that this mapping is not conformal for $s_x \neq s_y$ but adapts to the elongated structure of finger ridges: we already mentioned that they are rather elliptical around the finger tip – this in a way reflects the fact that fingers are longer than they are wide. Secondly, we allow for rotations of the finger by setting

$$(2.25)\qquad z'' = R_\theta(z') = e^{i\theta}\ z',$$

with $\theta \in [0, 2\pi)$, and finally we incorporate translations with

$$(2.26)\qquad w = T_m(z'') = z'' + m$$

for $m \in \mathbf{C}$. Thus we consider the orientation fields generated by the quadratic differentials $\sigma_{\text{basic},k}$ and σ_{circ} under the transformation

$$(2.27)\qquad w = F_{s_x,s_y,\theta,m}(z) = (T_m \circ R_\theta \circ S_{s_x,s_y})(z).$$

The transformed quadratic differentials are easily computed, cf. Equation (2.4); we omit the technical details. In the following we will, for ease of notation, denote the transformed models again by $\sigma_{\text{basic},k}$ and σ_{circ} ; it will be clear from the context whether they are considered in the z- or w-plane.

Remark 2.18. Note that $T_m \circ R_\theta$ directly models a Euclidean motion whereas one could say that S_{s_x,s_y} adapts to the size and thickness of the finger. If we fix a model $\sigma_{\text{basic},k}$ or σ_{circ}, we thus have five real parameters describing our model: s_x, s_y, θ, $\operatorname{Re} m$ and $\operatorname{Im} m$; here, we do not count the locations of the singular points as parameters since they are given and hence fixed. As any reasonable model should take the size and thickness of the finger, as well as possible translations and rotations, into account, one could argue that this parameter set contains a *minimal* number of parameters.

2.4. Review of existing models

We already discussed the model introduced by Sherlock and Monro (1993) in the previous section, see Equation (2.10) and Figure 2.2, where we have concluded that it is too simple to fit a given ridge pattern reasonably well. Note that it has only one free parameter, the orientation α at ∞. Several other authors built on this model though, trying to improve its accuracy. In the following we describe three such models we know of.

Recall that one can write the model of Sherlock and Monro (1993) for the orientation field ϕ as

$$\arg\phi(z) = \arg(\alpha^{-1}) + \sum_{i=1}^{2} \big(\arg(z - c_i) - \arg(z - d_i)\big) \mod 2\pi, \tag{2.28}$$

cf. Equation (2.9). Vizcaya and Gerhardt (1996) generalise this model by allowing for non-linear dependencies on the angles, i.e. they consider

$$\arg\phi(z) = \arg(\alpha^{-1}) + \sum_{i=1}^{2} \big(g_{c_i}(\arg(z - c_i)) - g_{d_i}(\arg(z - d_i))\big) \mod 2\pi, \tag{2.29}$$

where the continuous functions $g_{c_i}, g_{d_i} : [0, 2\pi] \to \mathbf{R}$ with $g_{c_i}(0) = g_{c_i}(2\pi)$, $g_{d_i}(0) = g_{d_i}(2\pi)$ have to be chosen such that no point's Poincaré index changes. In particular, Vizcaya and Gerhardt (1996) suggest to use piecewise linear functions with 8 evenly distributed knots. We summarise some of the properties of this model:

- In general, it cannot be represented by a quadratic differential.
- It is only applicable for loops and whorls; Vizcaya and Gerhardt (1996) do not discuss arches at all, although these constitute the fingerprint class for which the model of Sherlock and Monro (1993) performs worst.
- Their model uses 20 real parameters for a loop, and 40 for a whorl.
- The parameters are not invariant under rotations or translations.
- If a singular point is close to the border of the observed fingerprint area, some of its parameters will be difficult to estimate.

A different approach has been taken by Gu et al. (2004) who model the real and imaginary parts of an orientation field ϕ separately. Their idea is to add flexibility by allowing the influence of a singular point to vary through the addition of weights depending on the distance from the singular point, and by modelling a background field by polynomials. In particular, they set

$$\begin{aligned}\operatorname{Re}\phi(z) &= w_p(z)\, p_{\mathrm{Re}}(\operatorname{Re} z, \operatorname{Im} z) + \sum_{i=1}^{2} \operatorname{Re}\Big(w_{c_i}(z)\, \tfrac{|z-c_i|}{z-c_i}\, Q_{c_i} - w_{d_i}(z)\, \tfrac{z-d_i}{|z-d_i|}\, Q_{d_i}\Big)\\ \operatorname{Im}\phi(z) &= w_p(z)\, p_{\mathrm{Im}}(\operatorname{Re} z, \operatorname{Im} z) + \sum_{i=1}^{2} \operatorname{Im}\Big(w_{c_i}(z)\, \tfrac{|z-c_i|}{z-c_i}\, Q_{c_i} - w_{d_i}(z)\, \tfrac{z-d_i}{|z-d_i|}\, Q_{d_i}\Big)\end{aligned} \tag{2.30}$$

where $Q_{c_i}, Q_{d_i} \in \mathbf{R}$ model the "charge" of the singular points with weights

$$\begin{aligned} w_{c_i}(z) &= \max\big\{1 - \tfrac{|z-c_i|}{R_{c_i}}, 0\big\},\\ w_{d_i}(z) &= \max\big\{1 - \tfrac{|z-d_i|}{R_{d_i}}, 0\big\}, \text{ and}\\ w_p(z) &= 1 - \sum_{i=1}^{2}(w_{c_i}(z) + w_{d_i}(z)),\end{aligned} \tag{2.31}$$

limiting the influence of each singular point to a circle of radius R_{c_i} or R_{d_i}, respectively; here, p_{Re} and p_{Im} are real, bivariate polynomials of degree n in each variable modelling the background field; Gu et al. (2004) suggest $n = 4$. The properties of this model can be summarised as follows:

- There will in general be no quadratic differential representing this model.
- The model uses 50 parameters for an arch, 52 for a loop and 54 for a whorl.
- The parameters of the background field are not invariant under rotations or translations though the weights and radii of influence are.

To our knowledge, the only other model which is generated by a quadratic differential has been proposed by Zhou and Gu (2004): they actually consider (in our terminology)

$$\frac{g(z)}{f(z)}\, Q_{c_1,c_2,d_1,d_2}(z)\ dz^2 \tag{2.32}$$

with complex polynomials f, g of degree 6. For computational reasons they simplify this model to

$$\sigma_{\mathrm{ZG}}(z, dz) = \frac{1}{f(z)}\, Q_{c_1,c_2,d_1,d_2}(z)\ dz^2. \tag{2.33}$$

Note that $\sigma_{\mathrm{basic},2}$ is contained in Equation (2.32) with the appropriate choices of f and g if model $\sigma_{\mathrm{basic},2}$ is rescaled isotropically, i.e. if $s_x = s_y$, cf. Section 2.3. For arches, $\sigma_{\mathrm{basic},2}$ is also a special case of σ_{ZG} (when isotropically rescaled), but not for loops and whorls as the mirrored deltas cannot be represented. Recalling the diminishing influence of singular points (Corollary 2.16) and taking the added flexibility into account, however, we see that in principal σ_{ZG} might be similar to $\sigma_{\mathrm{basic},2}$ – even for loops and deltas. The particular choice of f will play a large rôle, though, as we shall see in Section 3.5. We note some more properties of σ_{ZG}:

- It uses 13 real parameters, the coefficients of the complex polynomial f. (Observe that the modulus of $f(z)$ does not affect the corresponding orientation field; we can thus assume the lowest order coefficient to have modulus 1, say.)
- Its parameters are not invariant under rotations or translations.
- For σ_{ZG} to be reasonable, the zeros of f need to lie outside the fingerprint region; the model is thus ill-suited for extrapolation in its generality.
- The model does not allow for non-conformity of the field, whence it can only incorporate isotropic rescalings.

We conclude that the models described in this section all add flexibility to the model by Sherlock and Monro (1993), thus increasing its accuracy. But they do so by sacrificing the other goals we set ourselves in Section 1.2: invariance under Euclidean motions, low dimension, interpretability, and predictive power; note that none of them can be expected to be very accurate when used for extrapolation. For practical reasons and since they are the only other models based on quadratic differentials, we will, on an empirical basis, compare our newly proposed models $\sigma_{\mathrm{basic},k}$ and σ_{circ} only with models σ_{SM} and σ_{ZG}, cf. Section 3.5.

Chapter 3

Algorithms

For any of the models discussed so far to be applicable, its parameters must be estimated from a given orientation field. As it turns out, this is not a trivial task – except for the model of Sherlock and Monro (1993). The general idea is to minimise a cost-functional over the fingerprint domain, i.e. given an observed orientation field ϕ on a bounded domain D and a model ψ_p for an orientation field depending on some parameters $p \in P \subset \mathbf{R}^d$, we consider that parameter $\hat{p}$ which minimises the functional measuring the fit,

$$J_d(p) = \int_D d\big(\phi(z), \psi_p(z)\big)\,dz, \tag{3.1}$$

for some distance[1] d on S^1; examples are the arc-length

$$d_{\mathrm{arc}}(z_1, z_2) = \min\big\{|\arg z_1 - \arg z_2|,\ 2\pi - |\arg z_1 - \arg z_2|\big\}, \tag{3.2}$$

or the Euclidean distance on S^1, leading to least-squares minimisation,

$$d_{\mathrm{LS}}(z_1, z_2) = (z_1 - z_2)^2. \tag{3.3}$$

To ease its interpretation, we will subsequently measure the accuracy of the fit of an orientation field ψ obtained from some model to a given orientation field ϕ on the bounded domain D by their *average deviation* in degrees[2]

$$\mathrm{ad}(\psi, \phi) = \frac{180}{2\pi|D|} \int_D d_{\mathrm{arc}}\big(\phi(z), \psi(z)\big)\,dz \tag{3.4}$$

where $|D|$ denotes the Lebesgue measure of D.

For models $\sigma_{\mathrm{basic},k}$ and σ_{circ} it has been found empirically that J_d usually features many local minima, rendering standard minimisation techniques like steepest descent or similar methods unusable. Upon closer inspection, the main problem was found to be the Euclidean motion, more precisely the determination of the rotation. Once the parameter θ specifying the rotation had been fixed, all other parameters could be determined rather well using standard techniques, see Section 3.4. The rotation therefore ought to be determined differently; we propose algorithms tackling this problem in Sections 3.2 and 3.3. We also discuss how the models from the literature described in Section 2.4 can be fitted, see Section 3.5. We begin by describing the algorithms used to obtain the orientation field and singular points of a given fingerprint.

[1] Note that d need not be a metric, e.g. d_{LS} is the square of the Euclidean distance.

[2] Observe that we have 180 degrees in the numerator instead of 360 since we need to halve orientations to obtain geometrically valid measures of angles.

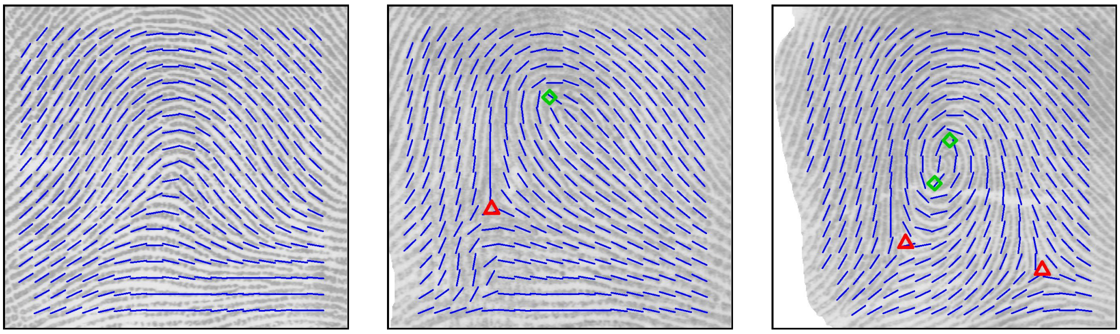

Figure 3.1. Orientation field and singular point extraction in the foreground of an arch, loop and whorl, respectively.

3.1. Extracting orientation fields and singular points

Given a fingerprint, we perform the following preparatory steps:

(1) segmentation of the image into the foreground containing the fingerprint pattern and the uninformative background,

(2) estimation of its orientation field in the foreground, and

(3) extraction of the singular points in the orientation field.

The segmentation step has been implemented using ideas proposed by Bazen and Gerez (2001) as well as Chen et al. (2004): few fingerprint images are segmented manually and used to train a linear classifier based on mean and variance of grey values of pixels in some window. Subsequently, this classifier is used to automatically segment the remaining images in the database. In a post-processing step, the boundary between fore- and background is smoothed by morphological operations (opening and closing).

The orientation field is most easily extracted by computing the gradients of the grey-scale image – which are vertical to the ridge boundaries –, square them (as complex values) to obtain orientations and rotate them by multiplication with -1. As these orientations are very noisy, they need to be smoothed which we have done by convolving with an isotropic Gaussian kernel, using FFT for efficiency. This is a variant of the widely-used method suggested by Bazen and Gerez (2002). Note that strong smoothing is necessary to avoid artificial singular points caused by noise, which may result in the translation of singular points. The latter is not a problem for our purposes, however, as we will not relate any orientation field back to the original image. In our empirical study, all models will be fit to the extracted, smoothed orientation field with its corresponding singular points, thus receiving equal data. Since their accuracy is evaluated against this smoothed orientation field, one might argue that the results obtained depend on the smoothing applied. Note however, that there is no such thing as *the* orientation field of a fingerprint, i.e. there is no “ground truth” to compare with: smoothing always is necessary and its amount reflects the scale at which we look at the orientation field. Figure 3.1, though, shows that we do not oversmooth but arrive at field reasonably reflecting the ridges’ flow, which can well be accepted for our purposes. Further note that due to the rigidity of the models we are going to consider, the amount of smoothing plays only a minor rôle when comparing these models one to another. Finally, observe that we only retain values having a certain distance from the boundary to make sure that the smoothed orientation field is based only on the foreground.

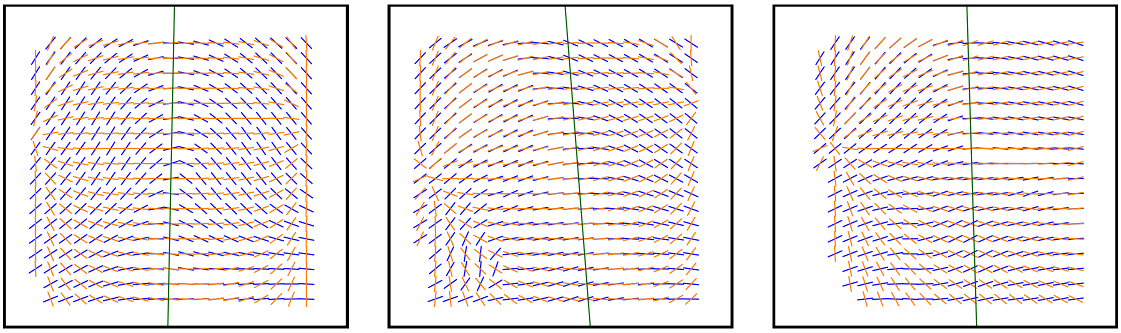

(a) (b) (c)

Figure 3.2. Lifted (except for the arch) orientation fields (blue), orientations of their gradients (orange), and resulting symmetry axes (green) using algorithm `small` for an arch, loop and whorl, respectively.

Bazen and Gerez (2002) also proposed an elegant method for determining the singular points based on the Poincaré index, see Definition 2.3. Instead of calculating the curve integral, they use Green's Theorem to turn it into an integral over a small area, which can again be computed very efficiently.

Figure 3.1 shows three sample images for which these steps have been taken. Note that the singular points have been moved slightly, and that despite the strong smoothing the orientation field in the lower left of the loop could not be well estimated. To the left of the whorl, the removal of the background is visible. Nonetheless, the flow of the fingerprint ridges has been captured rather well throughout the foreground of the images.

3.2. Determining the symmetry axis locally

We start by observing that the global or background field generated by σ_k is symmetric to the imaginary axis, see Equation (2.17) and Figure 2.3. As this is the field for an arch of models $\sigma_{\text{basic},k}$ or σ_{circ}, we aim to find such a symmetry axis in the orientation field of an arch, cf. Figure 3.1.

Clearly, the orientation field is orthogonal to such a symmetry axis, meaning it is constant along this axis. Thus any change of the orientation field close to the symmetry axis can only occur orthogonal to the axis, or parallel to the orientation field itself. To measure the change of the orientation field ϕ, we first *unwrap* ϕ, i.e. we write

$$\phi(z) = e^{iu(z)} \tag{3.5}$$

for some smooth $u : D \to \mathbf{R}$. Note that such a function u does exist iff the orientation field ϕ on D has no singular points (in D). Identifying $D \subset \mathbf{C}$ with a subset of $\mathbf{R}^2$ we can define a differential operator L which measures the change of ϕ at some point $z \in D$ by

$$L\phi(z) = -i\,\nabla \log \phi(z) = \nabla u(z) \in \mathbf{C}. \tag{3.6}$$

Note that $L\phi$ does not depend on the particular choice of u as two such functions differ only by a constant. We now may say that ϕ is *first-order symmetric* at z if $L\phi(z)$ is parallel to $\phi(z)$, i.e. if there is some $c \geq 0$ such that $\big(L\phi(z)\big)^2 = c\,\phi(z)$.

Figure 3.2(a) shows the orientation field ϕ of an arch overlaid by the orientation field of its change, $\big(L\phi(\cdot)\big)^2 / \big|\big(L\phi(\cdot)\big)^2\big|$. The parallelism of the orientations along the symmetry axis is clearly visible. To determine the orientation of the symmetry axis, recall that it is orthogonal to the orientation field there. We therefore simply take the mode of $-\phi(z)$ at all points z for which ϕ is first-order symmetric as the orientation of the axis. We then choose among all lines

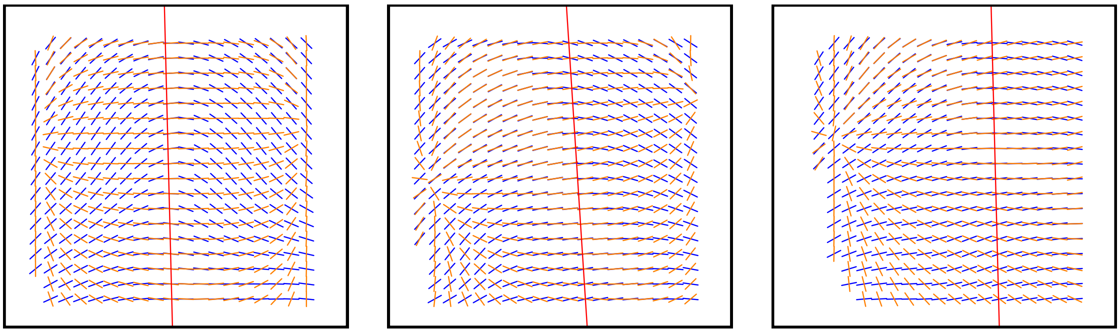

Figure 3.3. Strongly smoothed and lifted (except for the arch) orientation fields (blue), orientations of their gradients (orange), and resulting symmetry axes (red) using algorithm `large` for an arch, loop and whorl, respectively.

with that orientation the one along which most such points z lie. The resulting symmetry axis is again visualised in Figure 3.2(a).

Although this approach works reasonably well for arches, its application to loops and whorls is hampered by the fact that their "symmetry axis" is not visible in the central area of the fingerprint which usually constitutes the main part of the finger we observe, but "hidden" under the field created by the singular points, cf. Figure 3.1. However, we expect the outer or background field to be symmetric. Recall that in Section 2.3 we started by modelling the background field and then added the singular points by multiplying the corresponding quadratic differential with Q_{c_1,c_2,d_1,d_2}, cf. Equation (2.18). We thus can uncover the background field by reversing this step, i.e. by considering

$$(3.7) \qquad \psi(z) = \frac{Q_{c_1,c_2,d_1,d_2}}{|Q_{c_1,c_2,d_1,d_2}|}\,\phi(z).$$

Note that ψ no longer has any singular points: we *lifted* the singular points from ϕ. This operation was already used by Sherlock and Monro (1993) to obtain an orientation field free of singular points which can be unwrapped, cf. Equation (3.5); they then used this in order to interpolate orientation fields.

After lifting the singular points and obtaining the background field ψ, we can continue as before, unwrap the field using Equation (3.5), compute its change $L\psi$, check where it is parallel to ψ and determine the symmetry axis, see Figure 3.2(b) and (c). This is the method used in Huckemann et al. (2006).

Remark 3.1. This approach does not lead to the background field we envisaged, though: the mirrored singular points introduced in Equation (2.19) have not been lifted as this would have required knowledge about the horizontal axis – the information we were looking for in the first place. In practice, we can ignore this problem, however, as Corollary 2.16, further supported by empirical observations, shows.

The described approach has one drawback: it aims to find a globally valid symmetry axis based only on local information, namely orientations and their changes, in a small neighbourhood; we hence call this algorithm `small`. A simple way to improve this is by further smoothing the (lifted) orientation field ψ prior to the computation of its changes. This way the notion 'first-order symmetric' is based on a larger area, and we call the resulting algorithm `large`. Figure 3.3 shows the corresponding results when it is applied to three sample fingerprints.

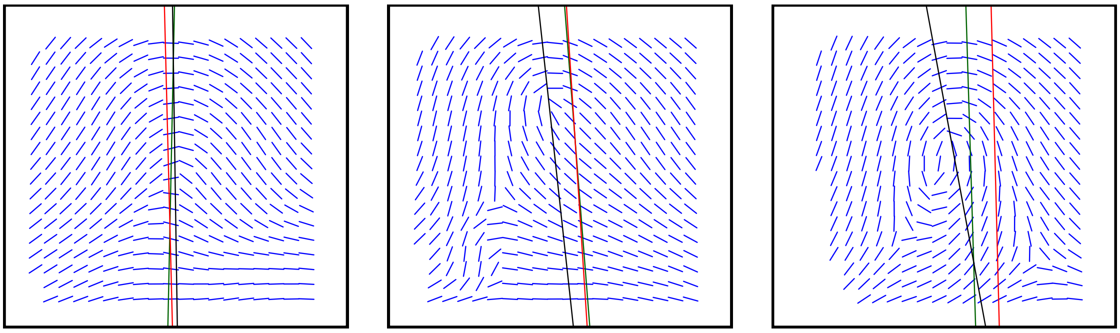

Figure 3.4. Orientation fields (blue) and corresponding symmetry axes extracted using algorithms `small` (green) `large` (red) and `energy` (black) for an arch, loop and whorl, respectively.

3.3. Determining the symmetry axis globally

Instead of a local characterisation of the symmetry axis as in Section 3.2 we now strive for a global one. We start by observing that an orientation field ψ on a domain D is symmetric w.r.t. the real axis iff

$$\psi(\bar{z}) = \overline{\psi(z)} \tag{3.8}$$

for all $z \in D \cap \bar{D}$ where $\bar{D} = \{\bar{z} \mid z \in D\}$. If we describe the symmetry axis by $\{s\alpha + ia\alpha \mid s \in \mathbf{R}\}$ through its orientation $\alpha^2 \in \mathrm{S}^1$ and its (signed) distance $a \in \mathbf{R}$ to the origin, then ψ is symmetric to this axis iff

$$\psi\big(\alpha(\overline{\alpha^{-1}z - ia} + ia)\big) = \alpha\overline{\alpha^{-1}\psi(z)} \tag{3.9}$$

or equivalently

$$\psi\big(\alpha(\overline{\alpha^{-1}z} + 2ia)\big)\alpha^{-2} \Big/ \overline{\psi(z)} = 1 \tag{3.10}$$

for all $z \in D \cap \bar{D}_{\alpha,a}$ where $\bar{D}_{\alpha,a} = \{\alpha(\overline{\alpha^{-1}z - ia} + ia) \mid z \in D\}$. We can now determine an optimal symmetry axis in the sense that it is the maximiser of the functional

$$A(\alpha, a) = \int_{D \cap \bar{D}_{\alpha,a}} \mathrm{Re}\left(\psi\big(\alpha(\overline{\alpha^{-1}z} + 2ia)\big)\alpha^{-2} \Big/ \overline{\psi(z)}\right) dz. \tag{3.11}$$

Note that we do not normalise by the area of $D \cap \bar{D}_{\alpha,a}$ to ensure that the optimal symmetry axis is based on a large part of D; otherwise one would obtain optimal results by placing the axis in a corner (e.g. the upper-right corner in Figure 3.4(a)) such that $D \cap \bar{D}_{\alpha,a}$ is a very small homogeneous area close to the axis.

To efficiently compute the maximiser of A we fix α and subsample $D \cap \bar{D}_{\alpha,a}$ on a regular grid rotated by $i\alpha$. The integral in Equation (3.11) along horizontal lines then conveniently becomes a convolution in dependence of a. It thus can be evaluated efficiently using FFT for all admissible values a leaving $D \cap \bar{D}_{\alpha,a}$ non-empty. This allows to quickly obtain the optimal value $\hat{a}$ for a given α. Note that subsampling barely reduces the accuracy of the method since the orientation field ψ is smooth.

To obtain the optimal $\hat{\alpha}$ we numerically optimise $A(\alpha, \hat{a}(\alpha))$ over $\arg\alpha \in [-\frac{\pi}{3}, \frac{\pi}{3}]$ (larger rotations do not occur in practice). We chose procedure `optimise` implemented in R (R Development Core Team 2006), a combination of golden section search and successive parabolic interpolation based on algorithm `localmin` by Brent (1973). We call the resulting algorithm for globally determining the symmetry axis `energy` as it is based on maximising the “energy” functional A.

Symmetry axes as determined by all three algorithms `small`, `large` and `energy` are shown in Figure 3.4 for three sample fingerprints. Note that the symmetry axis of the arch could easily be extracted as its orientation field showed a clear symmetry; this task was more difficult for loop and whorl where the axes differ considerably. The best axes arguably have been found by algorithm `energy` as they are well centred and seem to best reflect the behaviour of the outer field, especially for the whorl. Note that this algorithm has another advantage over algorithms `small` and `large` based on the local behaviour of the field: it does not require the symmetry axis to be observed as long as $D \cap \bar{D}_{\alpha,a}$ is not empty. This property will prove vital for prediction of areas covering the symmetry axis, see Section 4.2.

3.4. Fitting the newly proposed models

Once the symmetry axis has been found using any of the methods described in Sections 3.2 and 3.3, fitting models $\sigma_{\text{basic},k}$ and σ_{circ} proposed in Section 2.3 is straightforward. Recall that they depend on 5 real parameters, 3 of which describe the Euclidean motion and 2 the rescaling along the axes. The symmetry axis then leaves only one parameter free for the Euclidean motion, namely the position of the horizontal axis. We are therefore left with determining this as well as both rescaling parameters. Empirically it has been found that optimal values for these three parameters can efficiently be obtained using standard numerical optimisation techniques for the minimisation of the functional measuring the fit in Equation (3.4). We decided to use method `Nelder-Mead` of procedure `optim` implemented in R (R Development Core Team 2006) which is based on the simplex-method described by Nelder and Mead (1965), cf. also (Jarre and Stoer 2004, Section 17.1). Although we cannot guarantee a global minimum, our results obtained for a large amount of fingerprints show that the algorithm in the vast majority of cases converges to a sensible minimum, independent from the (reasonably chosen) starting values, see Chapter 4.

Results obtained when using the symmetry axes found by algorithm `energy` from Section 3.3 are shown for three sample fingerprints in Figure 3.5 which should be compared to the orientation fields obtained using models σ_{SM} and σ_{ZG}, see Figure 3.6. Note how well the newly proposed models fit the outer field, especially of the arch. Furthermore, all these models extrapolate reasonably well beyond the observed fingerprint domain. Table 3.1 reports the corresponding average deviations, cf. Equation (3.4). As expected, the fit improves if singular points are present since the field in the centre can then quite accurately be modelled by Q_{c_1,c_2,d_1,d_2}, while the background field constituting an arch is more difficult to model.

3.5. Fitting existing models

To find the optimal value of α, the orientation at ∞ in the model of Sherlock and Monro (1993), cf. Equation (2.10), we first observe that for any translation invariant distance d

$$J_d(\alpha) = \int_D d\big(\psi(z), \alpha\big) dz \tag{3.12}$$

where ψ is the orientation field where the singular points have been lifted, cf. Equation (3.7). For $d = d_{\text{LS}}$ the optimal α is thus the mean angle known from directional statistics, see e.g. (Mardia and Jupp 2000), which can efficiently be computed by projecting the ordinary mean of ψ over D (as a value in $\mathbf{C}$) and projecting it back onto S^1.

The models by Vizcaya and Gerhardt (1996) and Gu et al. (2004) both require numerical optimisation to be fit as the respective authors note. Since these models' aims and derivations differ strongly from our own considerations, we have not taken up the task to provide for efficient implementations of these models ourselves but excluded them from our numerical studies since no other implementations of these models were available to us, cf. Section 2.4.

Figure 3.5. Orientation fields (orange) of models $\sigma_{\text{basic},2}$ (top row), $\sigma_{\text{basic},4}$ (second row), $\sigma_{\text{basic},6}$ (third row), and σ_{circ} (bottom row), fit to an orientation field (blue) of an arch (left column), loop (middle column) and whorl (right column) where the symmetry axes (black) have been obtained using algorithm `energy`.

fingerprint	$\sigma_{\text{basic},2}$	$\sigma_{\text{basic},4}$	$\sigma_{\text{basic},6}$	σ_{circ}	σ_{SM}	σ_{ZG}
arch	11.9	11.2	10.9	11.9	32.1	19.1
loop	7.9	7.3	7.3	8.9	21.3	11.9
whorl	8.6	8.4	8.3	7.8	15.0	9.0

Table 3.1. Average deviations for the orientation fields shown in Figures 3.5 and 3.6.

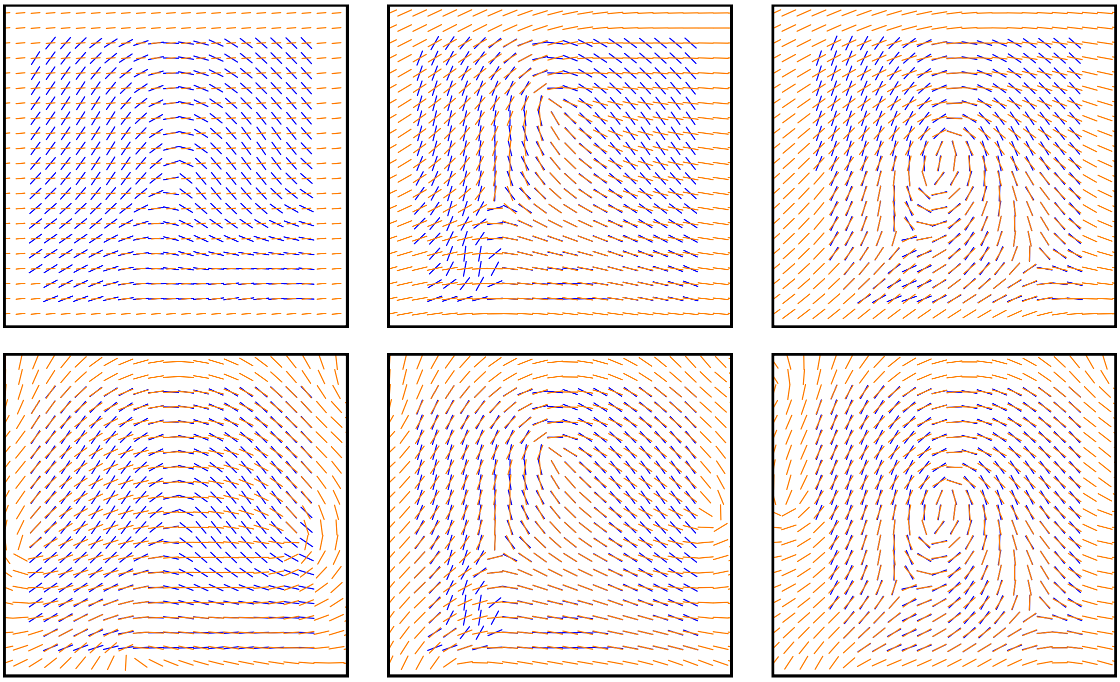

Figure 3.6. Orientation fields (orange) of models σ_{SM} (top row), and σ_{ZG} (bottom row), fit to an orientation field (blue) of an arch (left column), loop (middle column) and whorl (right column).

Zhou and Gu (2004) suggest to fit their model σ_{ZG} by ordinary least squares, i.e. instead of minimising J_d they suggest to minimise

$$\int_D |f(z) - \psi(z)|^2 dz \tag{3.13}$$

over all complex polynomials f of degree 6, cf. Equation (2.33); here, ψ is again the orientation field after lifting the singular points. Although being computationally efficient, this will in general not be equivalent to minimising $J_{d_{\text{LS}}}(f)$. Comparing to the optimisation for model σ_{SM} above, where α can be viewed as a complex polynomial of degree 0, here the projection step is missing. Thus $f(z)$ will be forced to be close to $\psi(z)$ not only in its argument but also in its modulus. Hence $f(z)$ will be close to 1 throughout D, strongly restricting the choices for f in the class of complex polynomials f of degree 6. We have nonetheless implemented model σ_{ZG} this way but note that there is no longer any reason to assume that it is close to or even better than any of the models we proposed in Section 2.3, cf. the discussion in Section 2.4.

Results of models σ_{SM} and σ_{ZG} fitted to three sample fingerprints are shown in Figure 3.6. The overly simple nature of model σ_{SM}, especially for arches is well visible as is the introduction of spurious poles of model σ_{ZG} close to the observed fingerprint region. Note that σ_{ZG} is not able to capture the flow of the arches or the local distortions of the loop, possibly due to the artificial rigidity caused by the optimisation based on ordinary least squares. The corresponding average deviations can be found in Table 3.1, documenting again that an increase in the number of singular points improves the accuracy of the models. Note however the poor performance of both models for the arch.

Chapter 4

Applications

Although the models proposed in Section 2.3 seem very promising when applied to some sample fingerprints as in Figure 3.5, their quality and usability can only be fairly judged based on analyses using a large number of automatically processed fingerprints. To measure the precision of our newly proposed models and to explore their potential for future applications we thus conducted a comparative field study where we used the NIST Special Database 4 (Watson and Wilson 1992) comprising a total number of 4000 images, 2 imprints each of 2000 distinct fingers equally distributed between the fingerprint classes arch, tented arch, left loop, right loop, and whorl (i.e. 400 fingers each). The original images were 512 pixels wide and 480 pixels high. We chose this database since: it is publicly available, thus allowing for future comparisons with our present results; its size allows to draw reasonable conclusions from our analyses; all fingerprint classes are well represented; and its images show a realistic variation of image quality. We initially also tried to use database 2a from (Maio et al. 2002) but found it inappropriate since its fingerprints rarely showed all singular points, cf. the discussion in Section 4.1; qualitatively the results obtained using that database were very similar. The computations were finally carried out on four personal computers of different configurations, in total lasting for about four days on each machine.

The images were initially segmented, and their background marked, by our colleague Krzysztof Mieloch using the methods described in Section 3.1. From these grey-scale images, orientation fields were extracted in the foreground and their singular points detected using the methods of Bazen and Gerez (2002), see Section 3.1. These orientation fields and singular points then served as the input for subsequent modelling and analyses.

The following questions guided our study:

(1) How accurate are our newly proposed models, in comparison to models from the literature?

(2) How robustly can these models be fitted?

(3) How well can they be used for inter- or extrapolation?

(4) How much information about the individual finger do the models' parameters contain?

The first two questions will be considered in Section 4.1, the third one in Section 4.2, whereas Sections 4.3 and 4.4 try to shed some light on the last question, each from a different perspective and with a different application in mind.

A word of caution before we proceed: the NIST Special Database 4 (Watson and Wilson 1992) has not been compiled to accurately resemble the distribution of fingerprints in the population, in particular it is unclear to which extent its fingerprints have been randomly sampled from a population, and whether different fingerprints belong to the same person. As mentioned above, all five fingerprint classes occur with equal frequencies in the database though their prevalences in the population vary strongly, arches e.g. are quite rare. Accordingly, we will report most results broken down into the different fingerprint classes. One then could combine the results from those classes with the according weights to obtain an overall measure of performance for the whole population, cf. (Maltoni et al. 2003, p. 191). Since the results can nonetheless not simply be generalised to a larger population due to the unknown sampling mechanism, and even more so since this particular database uses only one specific technique for acquiring fingerprints (namely digital scans of rolled ink-prints), we have refrained from computing such population level results. We will however use this database as a benchmark set of fingerprints, probably the best one publicly available, and interpret the results accordingly. We believe this is justified since we only look at *global* features at a *coarse* level – namely smoothed orientation fields and their singular points – whose essential variations within individual fingerprint classes might reasonably well be represented by such a large dataset. Results for the entire database will also be reported to allow for comparisons with other studies – but we caution once more against generalising such figures to infer about the population.

Before we state any results, we note that to the best of our knowledge this is the first comprehensive and openly verifiable study of models for orientation fields of fingerprints in the literature: Penrose (1969) gives no numerical results at all; Smith (1979) and Mardia et al. (1992) only show solutions for their differential equations for selected exemplary parameters; Kücken and Newell (2004) similarly show only results of some few simulations; Sherlock and Monro (1993) again give no numerical results; Vizcaya and Gerhardt (1996) use a total of 380 imprints stemming from 38 distinct loops and tented arches only which are not available for comparison; Gu et al. (2004) took a sample of 40 imprints from the NIST Special Database 14, and 60 imprints from an undisclosed source, without mentioning the distribution of images over fingerprint classes or the number of distinct fingers in either sample; and finally Zhou and Gu (2004) report results using 100 fingerprints of differing undisclosed sources including loops, whorls, twin loops and arches in unspecified frequencies stemming from an unstated number of distinct fingers. We thus deem it unreasonable to compare at face-value any of our results to any figures reported in the literature.

4.1. Accuracy

Arguably the first question, that needs to be answered when introducing a new model for some data, asks for the model's accuracy. To this end we fitted models σ_{SM}, σ_{ZG}, $\sigma_{\text{basic},2}$, $\sigma_{\text{basic},4}$, $\sigma_{\text{basic},6}$, and σ_{circ} to the extracted orientation fields, while using the obtained locations of their singular points. These models have been fitted as described in Chapter 3; algorithms `small`, `large` and `energy` were used to obtain a symmetry axis for the latter models, resulting in three different fits for each of these models.

Since all mentioned models require that the locations of *all* singular points be specified, we first checked for every orientation field whether the orders of its singular points summed to 0, cf. Remark 2.14, otherwise discarding that fingerprint. We also discarded the fingerprint if the foreground of the image constituted less than one third of the whole image's area. This left us with a total of 3357 images. Out of these, algorithm `small` failed to find a symmetry axis in 3, algorithm `large` in 6 cases when the orientation field was first-order symmetric at too few points; algorithm `energy` never failed. To ensure that all models were compared on

	$\sigma_{\text{basic},2+\texttt{opt}}$	$\sigma_{\text{basic},4+\texttt{opt}}$	$\sigma_{\text{basic},6+\texttt{opt}}$	$\sigma_{\text{circ}+\texttt{opt}}$	σ_{SM}	σ_{ZG}
all classes	9.7	8.9	8.8	8.9	22.3	13.6
arches	10.2	9.7	9.6	10.2	26.3	16.4
loops	9.8	8.9	8.8	8.8	22.2	13.4
whorls	7.0	6.8	7.0	6.9	14.0	8.5

Table 4.1. Average deviation for models $\sigma_{\text{basic},2}$, $\sigma_{\text{basic},4}$, $\sigma_{\text{basic},6}$, σ_{circ}, σ_{SM}, and σ_{ZG} reported as median over all fingerprints, as well as over arches, loops and whorls, respectively; models $\sigma_{\text{basic},k}$ and σ_{circ} have been fitted using algorithm `opt`.

the same set of fingerprints in this section, we report results only for the 3349 images for which all algorithms succeeded. Out of these, 757 were arches, 2146 loops (including tented arches), and 446 were whorls, according to the database's documentation. Unsurprisingly, the more singular points a fingerprint had the more difficult it was to find all of them, leaving us with just 55% of the whorls, still enough to draw reasonable conclusions though.

Recall that we aimed at finding the parameters of models $\sigma_{\text{basic},k}$ and σ_{circ} as global minimisers of the average deviation, cf. Equation (3.4), devising three algorithms for fixing the vertical axis as (sub-optimal) substitutes out of numerical necessities. If we were only interested in these models' *capabilities* we thus might want for each fingerprint to look at the optimal parameter sets obtained with *any* of these three algorithms, i.e. out of the three fits obtained for such a model we would choose the one with the lowest average deviation; the resulting algorithm will be called `opt`.

Figure 4.1 shows cumulative distribution functions for the resulting average deviations for all fingerprints and for the respective classes (arches, loops and whorls); corresponding medians[1] are reported in Table 4.1. Note that an increase in the number of singular points results in improved fits, especially so for models σ_{SM} and σ_{ZG}, as conjectured in Section 3.5. Clearly, the new models proposed in Section 2.3 outperform the other two models in terms of accuracy of the fit: the median average deviation is halved when compared to σ_{SM} and it is even an improvement of roughly 1.5 degrees for whorls over σ_{ZG}, up to over 6 degrees for arches; this is a remarkable achievement taking the much smaller number of parameters – 5 as opposed to 13 – into account.

The comparisons so far used algorithm `opt` which chooses the best fit from the three algorithms `small`, `large`, and `energy`. A natural question to ask is which of these algorithms actually gives the best fits and whether there is a single best algorithm. To this end we computed for each individual fingerprint the difference in fit between each pair of algorithms. The results differ only very slightly between different models and different fingerprint classes so we only present them for model σ_{circ} and for all fingerprints, see Table 4.2. Apparently, algorithm `energy` improves upon the other algorithms in about two-thirds of the fingerprints, although the median improvement is small. Possibly more importantly, it is also the most robust of the algorithms considered, leading to misfits with large average deviations only in very few cases, see Table 4.3. Another useful way to compare algorithms is by their runtime: algorithm `small` took an average of 0.045 seconds to find a symmetry axis, algorithm `large` needed 5.7s and algorithm `energy` 6.1s. Note that none of these algorithms has been optimised for speed though. Algorithm `small` is much quicker as it does not require the computation of any further convolutions, algorithm `energy` is however only slightly slower than `large`. Taking all this into account and observing its wider applicability, cf. Section 3.3, algorithm `energy` appears to be our best choice, and we will mainly consider this algorithm

[1]Note that we report medians instead of means since the distributions of the average deviation over the fingerprints are skewed as is visible in Figure 4.1.

difference	$q_{0.05}$	$q_{0.25}$	median	$q_{0.75}$	$q_{0.95}$	prop. > 0
`small` − `large`	-1.5	-0.2	0.1	0.5	4.2	57.8%
`small` − `energy`	-1.4	-0.2	0.5	1.7	7.1	68.2%
`large` − `energy`	-1.4	-0.2	0.3	1.3	5.6	65.3%

Table 4.2. Distribution (5%, 25%, 75%, 95%-quantiles, median and proportion above 0) over all fingerprints of pairwise differences in average deviation between algorithms `small`, `large` and `energy`, for model σ_{circ}.

tail of av. dev.	$\sigma_{\text{basic},6+\texttt{small}}$	$\sigma_{\text{basic},6+\texttt{large}}$	$\sigma_{\text{basic},6+\texttt{energy}}$	$\sigma_{\text{circ}+\texttt{energy}}$	σ_{SM}	σ_{ZG}
prop. > 15 deg.	13.7%	9.6%	2.1%	3.2%	89.6%	38.3%
prop. > 20 deg.	5.8%	3.8%	0.5%	0.5%	65.6%	7.6%
prop. > 25 deg.	2.9%	2.1%	0.2%	0.3%	34.9%	0.3%

Table 4.3. Proportions out of all fingerprints which resulted in large ($>$ 15, 20, or 25 degrees) average deviations for different models and algorithms.

for the remainder of our study; cf. also to the discussion on the stability of the extracted axis in Section 4.4.

Now that we have singled out an algorithm to find the symmetry axis, subsequently allowing to fit models $\sigma_{\text{basic},k}$ and σ_{circ}, we repeat our analyses of comparing the fits obtained by the various models for the different fingerprint classes from the beginning of this section. The results when using algorithm `energy` instead of algorithm `opt` can be found in Figure 4.2 and Table 4.4 which should be compared to Figure 4.1 and Table 4.1. Although we see the expected slight decline in accuracy, the qualitative picture has not changed: the newly proposed models still outperform the others by a clear margin with σ_{ZG} only for whorls getting close. Note that they are even "uniformly" better than the others, in the sense that their cumulative distribution functions are uniformly larger. This is not to say that they are better for each individual fingerprint but that their best as well as their worst fits are more accurate than the ones of the others.

It also appears that although model $\sigma_{\text{basic},6}$ is best for modelling arches, model σ_{circ} is better for modelling loops and whorls, see Table 4.1. We can examine this more thoroughly by looking at the differences between the average deviations of these two models for individual fingerprints of the different fingerprint classes. Details of the corresponding distributions are given in Table 4.5, supporting the claim for arches and possibly whorls but showing no superiority of either model over the other for loops; both models also seem to be equally robust, cf. also Table 4.3. Since the only clear difference is for arches where $\sigma_{\text{basic},6}$ gives the best results, we will subsequently focus on this model.

We conclude this section by looking at some of the cases where model $\sigma_{\text{basic},6}$ based on algorithm `energy` failed: the average deviation of just 7 fingerprints was larger than 25 degrees, cf. Table 4.3. Out of these, 6 fingerprints had their singular points wrongly detected. Figure 4.3 exemplarily shows two such cases: the left figure has a core missed in the low-contrast background in the centre of the image, and a delta is outside the observed region further to the lower-right. Since both a core and a delta were missed their orders still summed to zero and the image was not excluded; note how model $\sigma_{\text{basic},6}$ tries to "recreate" the curvature around the missing core by placing its artificial poles close to the lower-left corner, producing steep hats at the upper right. The middle figure shows the more common case of one delta being missed (visible at the right border) and instead a spurious one being introduced due to noise (in the upper-left corner). In both cases, the lifted orientation fields

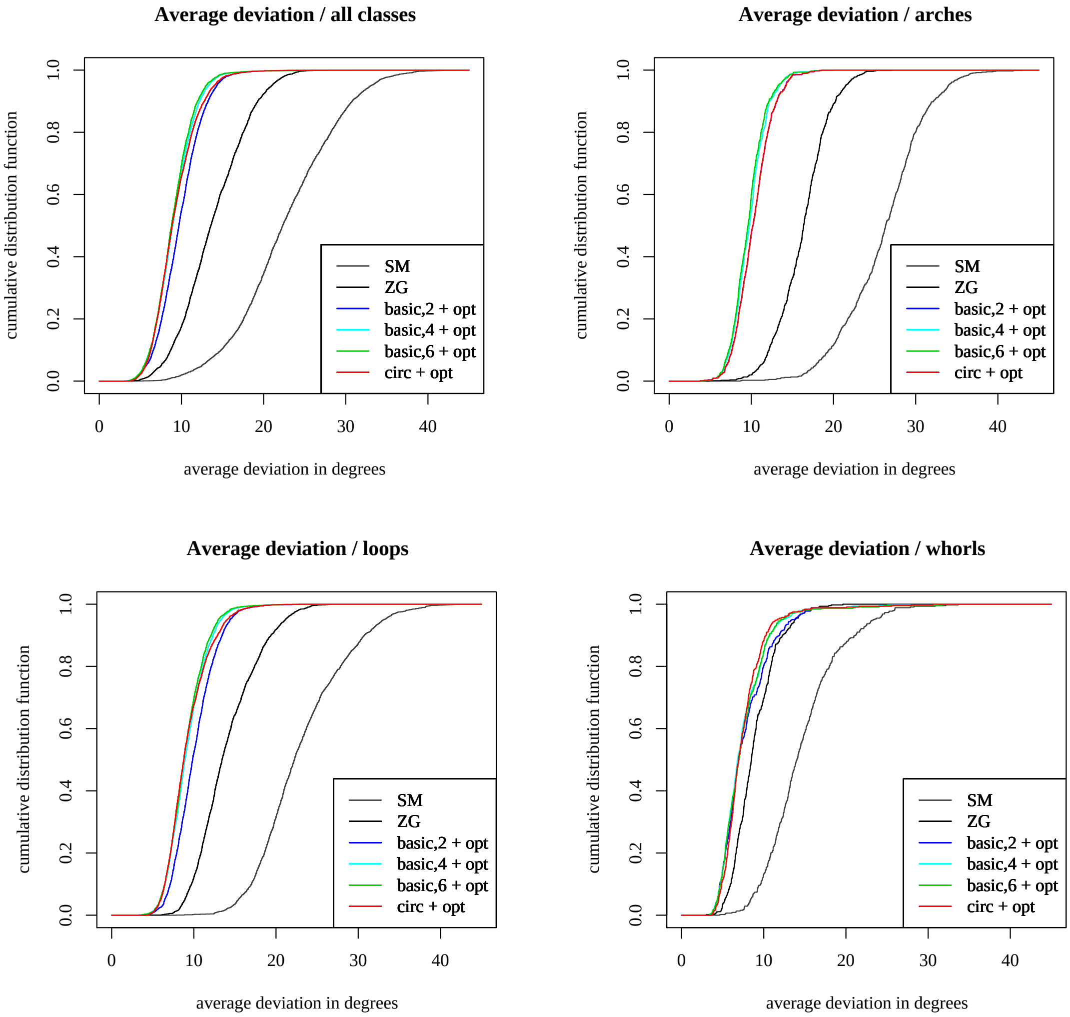

Figure 4.1. Cumulative distribution functions (empirical) of average deviation (in degrees) for models σ_{SM}, σ_{ZG}, $\sigma_{\mathrm{basic},2}$, $\sigma_{\mathrm{basic},4}$, $\sigma_{\mathrm{basic},6}$, and σ_{circ} over all fingerprint classes, as well as restricted to arches, loops and whorls, respectively; models $\sigma_{\mathrm{basic},k}$ and σ_{circ} have been fitted using algorithm `opt`.

	$\sigma_{\mathrm{basic},2+\mathtt{energy}}$	$\sigma_{\mathrm{basic},4+\mathtt{energy}}$	$\sigma_{\mathrm{basic},6+\mathtt{energy}}$	$\sigma_{\mathrm{circ}+\mathtt{energy}}$	σ_{SM}	σ_{ZG}
all classes	10.3	9.7	9.5	9.2	22.3	13.6
arches	10.4	10.0	9.8	10.4	26.3	16.4
loops	10.6	9.8	9.7	9.1	22.2	13.4
whorls	8.0	7.9	7.9	7.4	14.0	8.5

Table 4.4. Average deviation for models $\sigma_{\mathrm{basic},2}$, $\sigma_{\mathrm{basic},4}$, $\sigma_{\mathrm{basic},6}$, σ_{circ}, σ_{SM}, and σ_{ZG} reported as median over all fingerprints, as well as over arches, loops and whorls, respectively; models $\sigma_{\mathrm{basic},k}$ and σ_{circ} have been fitted using algorithm `energy`.

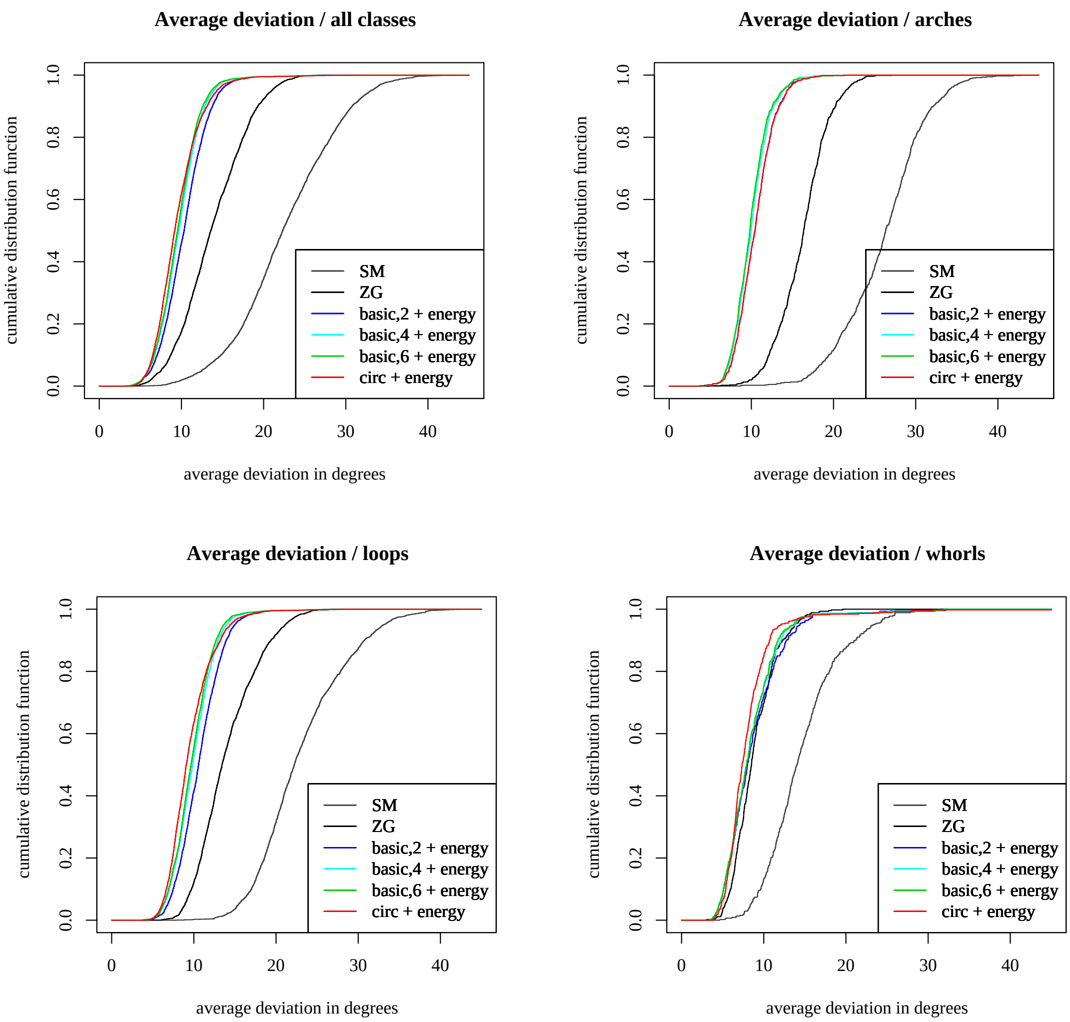

Figure 4.2. Cumulative distribution functions (empirical) of average deviation (in degrees) for models σ_{SM}, σ_{ZG}, $\sigma_{\mathrm{basic},2}$, $\sigma_{\mathrm{basic},4}$, $\sigma_{\mathrm{basic},6}$, and σ_{circ} over all fingerprint classes, as well as restricted to arches, loops and whorls, respectively; models $\sigma_{\mathrm{basic},k}$ and σ_{circ} have been fitted using algorithm `energy`.

fingerprint class	$q_{0.05}$	$q_{0.25}$	median	$q_{0.75}$	$q_{0.95}$	prop. > 0
all classes	-1.8	-0.9	-0.2	0.7	3.4	42.2%
arches	-1.7	-1.1	-0.6	0.0	0.6	24.3%
loops	-1.9	-0.9	-0.2	1.1	3.7	44.7%
whorls	-1.9	-0.3	0.2	1.1	3.5	60.8%

Table 4.5. Distribution (5%, 25%, 75%, 95%-quantiles, median and proportion above 0) over all fingerprints and for different fingerprint classes of pairwise differences in average deviation between models $\sigma_{\mathrm{basic},6}$ and σ_{circ}, the average deviations of the latter being subtracted from those of the former.

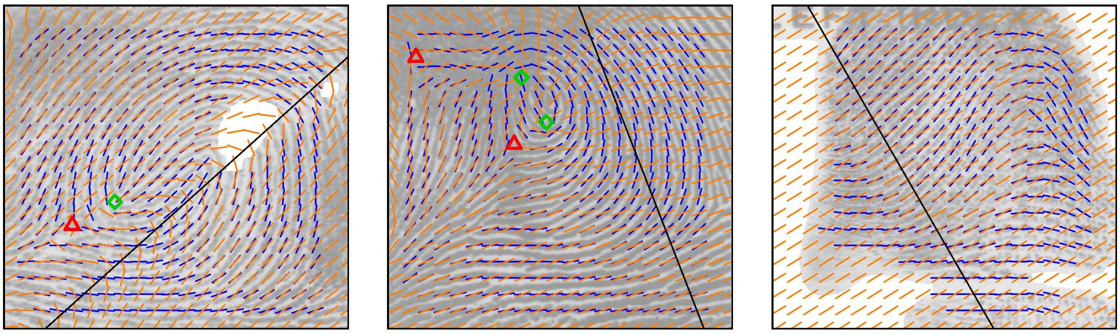

Figure 4.3. Orientation fields of model $\sigma_{\text{basic},6}$ (orange) fitted using the vertical axis found by algorithm `energy` (black) to some originally extracted orientation fields (blue) and singular points (Δ marks a delta, $\Diamond$ a core); left and middle figure show wrongly detected singular points, the right figure shows a misplaced axis; see page 31 for details.

do not show the required symmetry and the axes are misplaced. Note that none of the models considered could accurately model these fields. The right figure shows the only fingerprint with such an average deviation larger than 25 degrees where the problem was not caused by missed singular points: algorithm `energy` wrongly placed the symmetry axis too far to the left, essentially taking the curvature there to resemble the arch; note that the actual symmetry axis of that arch is supported only by a small region since it is so close to the border. Subsequently, model $\sigma_{\text{basic},6}$ averages between the opposing curvatures to the right of the chosen axis. Potentially, using a more sophisticated functional in Equation (3.11) might help to avoid such cases.

4.2. Prediction

One of the areas where orientation fields are applied in fingerprint analyses is for enhancing low-quality regions, cf. Section 1.2. However, it is also difficult to reliably extract an orientation field in those regions. Parametric models for orientation fields can be used to solve this problem by extrapolating the field fitted to the orientation field in high-quality regions into regions of lower quality. This might also be useful for matching as it allows to compare orientation fields even in low-quality regions. We have simulated this scenario by setting the contrast in some arbitrary region of the fingerprint to zero.

Starting from the 3357 images of Section 4.1 showing equally many cores and deltas, we randomly removed a 101×101 square from each image under the constraint that at least 70% of the square's area was in the foreground and no singular point was removed. We then filled the squares by mean grey, marked them as background and recomputed the corresponding orientation fields and their singular points, proceeding if there were as many cores and deltas as before. This left us with 3035 images. We then fitted models σ_{SM}, σ_{ZG}, $\sigma_{\text{basic},2}$, $\sigma_{\text{basic},4}$, $\sigma_{\text{basic},6}$, and σ_{circ} to those orientation fields, using algorithm `energy` for the latter models. Finally we extrapolated these fits into the squares and compared them to the originally extracted orientation fields by computing their average deviation there (over the corresponding squares). Let us note that out of those images considered, 745 were arches, 1931 loops (including tented arches), and 359 were whorls, according to the database's documentation.

Figure 4.4 exemplarily shows three orientation fields of fingerprints where the square that has been cut out is marked; there, only the extrapolated orientation field (obtained using model $\sigma_{\text{basic},6}$) is available. Table 4.6 and Figure 4.5 summarise the average deviations for models σ_{SM}, σ_{ZG}, $\sigma_{\text{basic},2}$, $\sigma_{\text{basic},4}$, $\sigma_{\text{basic},6}$, and σ_{circ} for all fingerprints and broken down into the different fingerprint classes; these results should be compared to Table 4.4 and Figure 4.2.

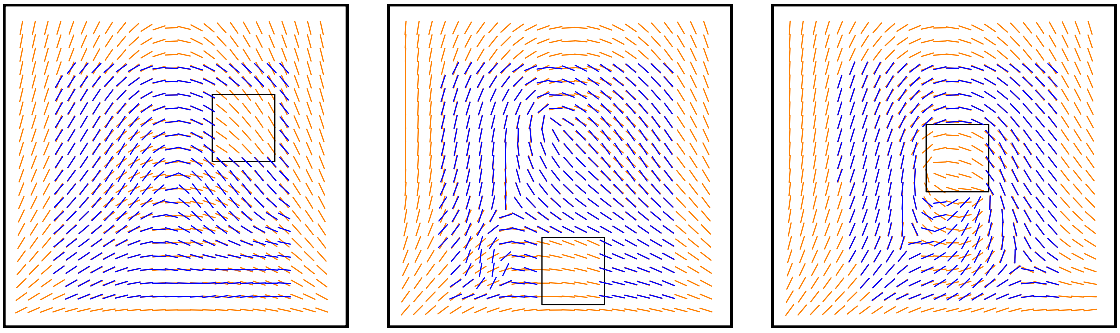

Figure 4.4. Orientation fields of model $\sigma_{\text{basic},6}$ (orange) fitted to the orientation fields (blue) extracted from fingerprints where a 101×101 pixel square (black) has been cut out.

Note that prediction gets more difficult when there are more singular points – which seems counter-intuitive as the opposite behaviour was observed for the accuracy of the fit. A possible explanation lies in the increased difficulty to detect all singular points correctly, especially since they are allowed to be arbitrarily close to the removed region. An example of this effect can be seen in Figure 4.4 where the square was cut out so close to the cores of the whorl that they have been misplaced afterwards. Still, the newly proposed models achieve much better predictions than models σ_{SM} and σ_{ZG}.

4.3. Variation of the parameters

There are several reasons why one might be interested in measuring how much parameters vary between different imprints of the same finger:

Stability: it allows us to measure how stable the extracted parameters remain under Euclidean motions, partial observations, etc., cf. Section 1.1.

Information content: the amount of information the parameters contain about individual fingers can be quantified as the variation of the parameters for different imprints of a single finger relative to the variation of the parameters in the whole population.

Indexing: the less parameters vary between different imprints of the same finger when compared to their variation in the population the greater the savings can be if they are used as database indices.

Recall that the only parameters that can be expected to be invariant under Euclidean motions are the scaling parameters s_x and s_y of models $\sigma_{\text{basic},k}$ and σ_{circ} whilst none of the parameters of models σ_{SM} and σ_{ZG} has this property. For simplicity, we will report results only for model $\sigma_{\text{basic},6}$, cf. the discussion in Section 4.1.

One could argue from their definition that s_x measures the width of a finger whereas s_y measures its height. We can thus derive measures of the size as well as of the thickness (or rather "thinness") of the finger, namely

$$s_p = s_x s_y \quad \text{and} \quad s_r = s_y / s_x, \tag{4.1}$$

respectively. Note that s_r also measures the non-conformity of the model's quadratic differential, cf. Section 2.3.

Since all parameters in question are *scaling* parameters it is natural to take their logarithms prior to analysis, we thus consider

$$l_x = \log_{10} s_x \quad l_y = \log_{10} s_y \quad l_p = \log_{10} s_p \quad \text{and} \quad l_r = \log_{10} s_r. \tag{4.2}$$

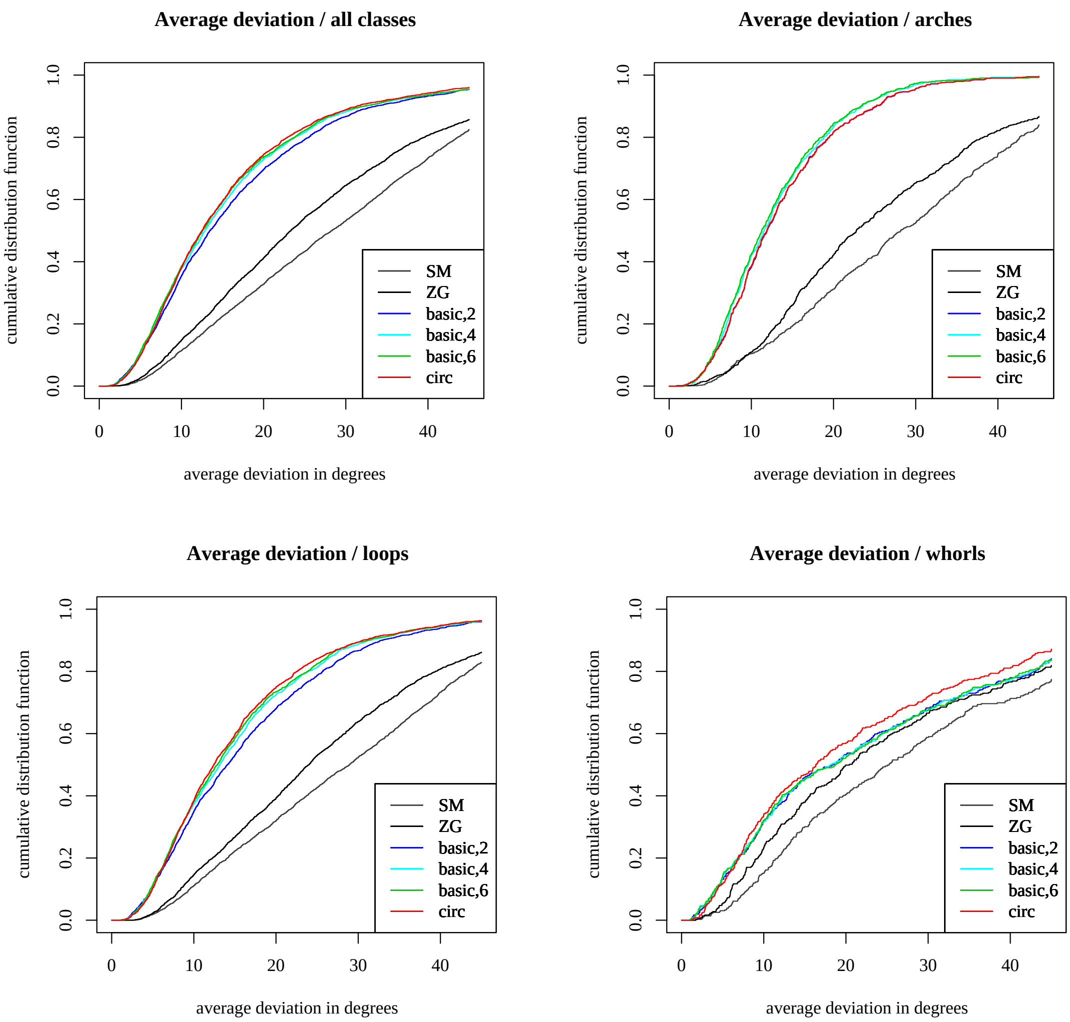

Figure 4.5. Cumulative distribution functions (empirical) of average deviation (in degrees) of the extrapolated orientation fields of models σ_{SM}, σ_{ZG}, $\sigma_{\mathrm{basic},2}$, $\sigma_{\mathrm{basic},4}$, $\sigma_{\mathrm{basic},6}$, and σ_{circ} from the originally extracted orientation fields on the predicted squares, over all fingerprint classes, as well as restricted to arches, loops and whorls, respectively; models $\sigma_{\mathrm{basic},k}$ and σ_{circ} have been fitted using algorithm `energy`.

	$\sigma_{\mathrm{basic},2}$	$\sigma_{\mathrm{basic},4}$	$\sigma_{\mathrm{basic},6}$	σ_{circ}	σ_{SM}	σ_{ZG}
all classes	13.5	12.9	12.6	12.5	28.3	23.3
arches	11.9	11.6	11.3	11.9	28.2	22.8
loops	14.1	13.2	12.9	12.4	28.9	24.0
whorls	18.4	18.1	18.7	16.3	25.2	20.4

Table 4.6. Average deviations of the extrapolated orientation fields of models $\sigma_{\mathrm{basic},2}$, $\sigma_{\mathrm{basic},4}$, $\sigma_{\mathrm{basic},6}$, σ_{circ}, σ_{SM}, and σ_{ZG} from the originally extracted orientation fields on the predicted squares, reported as median over all fingerprints, as well as over arches, loops and whorls, respectively; models $\sigma_{\mathrm{basic},k}$ and σ_{circ} have been fitted using algorithm `energy`.

To obtain a justifiable quantification of the parameters' variation, we need a probabilistic model for the observed parameter values. It appears most reasonable to employ a so-called *random-effects model* in our situation, i.e. we assume that there is a "mean" parameter value ζ_i for finger i around which the observed parameter value $Z_{i,j}$ of imprint j of this finger will be distributed. To be more precise, assume we are interested in some parameter which we observed (e.g. l_x), denoting the observed values by $Z_{i,j}$ where i denotes the number of the finger and j the number of its imprint for which we observed this particular value; we then assume that there are i.i.d. random variables ζ_i with mean μ and variance $\sigma_b^2 < \infty$ and, independent of these, i.i.d. random variables $\epsilon_{i,j}$ with mean 0 and variance $\sigma_w^2 < \infty$ such that

$$(4.3) \qquad Z_{i,j} = \zeta_i + \epsilon_{i,j}.$$

σ_b then measures the parameter's variation *between* different fingers, σ_w its variation *within* the same finger, i.e. between its different imprints. The ratio σ_b/σ_w between these variations then provides us with a quantification of the parameter's variation between different fingers in terms of its variation within a single finger. If this quantity is small (close to 0) the parameter's value (on average) contains very little information about the individual finger, if it is large (larger than 1), however, then the parameter is quite informative.

Since the database we used only contains two imprints per finger, we cannot easily check the assumptions made, especially the ones about the identical distribution of the random variables $\epsilon_{i,j}$ and their independence from random variables ζ_i. We will thus use them only as "working assumptions", taking care when interpreting the corresponding results, cf. also the discussion on page 29. As we cannot directly observe σ_b/σ_w, we need to estimate it. To this end we consider for each finger i

$$(4.4) \qquad B_i = \frac{Z_{i,1} + Z_{i,2}}{2}$$

which might be viewed as a predictor for ζ_i, as well as

$$(4.5) \qquad W_i = \frac{Z_{i,1} - Z_{i,2}}{2}$$

whose distribution is independent of ζ_i. More precisely we have the following simple

Lemma 4.1. *Under the above assumptions,*

$$(4.6) \qquad \operatorname{Var} W_i = \frac{\sigma_w^2}{2} \quad \text{and} \quad \operatorname{Var} B_i = \sigma_b^2 + \frac{\sigma_w^2}{2}$$

identically for all i.

We thus could estimate σ_b/σ_w by

$$(4.7) \qquad \sqrt{\operatorname{var} B - \operatorname{var} W} \Big/ \sqrt{2 \operatorname{var} W}$$

where $\operatorname{var} B$ is the empirical variance of the B_i, $\operatorname{var} W$ accordingly of the W_i. Since the parameters we are considering cannot be assumed to be normally distributed but might have heavy tails, we instead use the more robust

$$(4.8) \qquad \rho = \sqrt{\mathrm{IQR}(B)^2 - \mathrm{IQR}(W)^2} \Big/ \sqrt{2}\, \mathrm{IQR}(W)$$

as our *ratio of variation* where $\mathrm{IQR}(B)$ denotes the *interquartile range* of the B_i and $\mathrm{IQR}(W)$ accordingly of the W_i.

This quantity can easily be computed for the parameters we are interested in, i.e. for l_x, l_y, l_p and l_r, giving us four ratios of variation, ρ_x, ρ_y, ρ_p and ρ_r, respectively. Table 4.7 summarises them for the parameters obtained using model $\sigma_{\text{basic},6}$ with algorithm `energy` for all fingerprints and when computed for each class of fingerprints individually. To obtain

fingerprint class	ρ_x	ρ_y	ρ_r	ρ_p
all classes	1.77	5.83	9.40	4.00
arches	0.90	1.23	1.13	1.11
loops	1.72	2.73	4.06	2.32
left loops	1.68	1.44	1.95	1.37
right loops	1.46	1.50	1.74	1.44
tented arches	1.36	4.00	4.19	3.06
whorls	1.89	2.37	2.36	2.21

Table 4.7. Ratios of variation for different scaling parameters of model $\sigma_{\text{basic},6}$ fitted using algorithm `energy`.

this table we used 1525 *pairs* of images for which equally many cores and deltas were found; according to the database's documentation these were 360 arches, 984 loops (comprising 315 left loops, 320 right loops, and 349 tented arches) as well as 181 whorls. The figures indicate that there clearly is information contained in the parameters, most notably in l_r – this might have been expected: the outer orientation field created by model $\sigma_{\text{basic},6}$ changes relatively little when s_x and s_y are modified simultaneously as compared to the change induced by modifying their ratio. Note that most of the variation between different fingers seems to be due to those fingers belonging to different classes (which is why we have additionally broken the loops down into their classical categories) though still considerable information seems to be present in the parameters of those fingerprints other than arches, especially of tented arches. Observe that the high ratios of variation for all fingerprints also allow us to infer that the parameters s_x and s_y vary relatively little between different imprints of the same finger when compared to their variation between different fingers, in other words they remain relatively stable when another imprint of the same finger is taken.

To explore the potential usefulness of these parameters for database indexing we conducted the following experiment emulating a scenario in which a given finger is to be identified in the database: for each finger i we took the parameter value $Z_{i,1}$ of its first imprint representing the fingerprint obtained whose match we are trying to find among the second imprints representing the database. We accordingly sorted the second imprints of all fingers j by $|Z_{j,2} - Z_{i,1}|$. The rank of $|Z_{i,2} - Z_{i,1}|$ in this sequence then tells us how many imprints in the database we would need to look through until we found the match. Note that on average we would need to look through half of the images if the sequence was purely random, the corresponding standard deviation would amount to about 28.9%.

The results of this experiment for our parameters of interest are summarised in Table 4.8. Again we see that most of the gain obtained when scanning through all images is due to the parameter values differing considerably between the different classes. Note also the large standard deviations, indicating that at times large proportions of the database had to be scanned. Nonetheless quite remarkable speed-ups seem to be possible for loops and whorls when sorting according to parameter l_r.

fingerprint class	l_x	l_y	l_r	l_p
all classes	0.31 (0.26)	0.28 (0.26)	0.25 (0.25)	0.29 (0.27)
arches	0.40 (0.28)	0.44 (0.28)	0.43 (0.28)	0.44 (0.28)
loops	0.31 (0.26)	0.32 (0.27)	0.26 (0.26)	0.33 (0.28)
left loops	0.33 (0.27)	0.34 (0.27)	0.28 (0.26)	0.36 (0.28)
right loops	0.33 (0.27)	0.37 (0.29)	0.31 (0.27)	0.37 (0.29)
tented arches	0.37 (0.28)	0.35 (0.28)	0.34 (0.28)	0.35 (0.28)
whorls	0.32 (0.27)	0.28 (0.25)	0.28 (0.22)	0.30 (0.26)

Table 4.8. Average proportion (and corresponding standard deviation) of second imprints to be scanned until the one corresponding to the first imprint is found, when sorted by similarity of the specified parameter of model $\sigma_{\text{basic},6}$; as appropriate the search has been restricted to the named fingerprint class. See Section 4.3 for details.

4.4. Intrinsic coordinates

As already mentioned in Section 1.2, a reliable way of defining intrinsic coordinates is very useful, e.g. for matching minutiae. We are now going to analyse how well the Euclidean motion determined while fitting model $\sigma_{\text{basic},6}$ can be used for this purpose. We start by examining how stable the orientation of the vertical axis is. In order to measure this, we need some reference points or axis. We thus restrict ourselves to loops and whorls and use the axis connecting a loop's core and delta as the reference axis, for whorls we use the barycentres of its cores and of its deltas, respectively. We then measure the angle between this reference axis and the axis obtained from any of the algorithms `small`, `large` and `energy`, and compare the angles obtained from both imprints of the same finger. For comparison we also interpret parameter α of model σ_{SM} as the orientation of a horizontal axis and compute its angle with the reference axis analogously. For 845 *pairs* of images one or two cores and equally many deltas were found in both images, while all algorithms we are considering succeeded; these were classified as 688 loops (comprising 273 left loops, 280 right loops, and 135 tented arches) as well as 157 whorls, according to the database's documentation. The medians of the differences in orientation (in degrees) obtained this way are reported in Table 4.9. Clearly, algorithm `energy` provides for a much more reliable symmetry axis than the others.

The next step was to compare x-coordinates of the barycentre of all singular points, which we used as a reference point, in each of the two imprints. Note that the computation of an x-coordinate only requires to fix a vertical axis whence this comparison does not depend on the particular model but only on the algorithm chosen; we can however no longer compare with model σ_{SM} as it does not specify an axis. Table 4.9 contains also the results of this step (reported as median differences in pixels), showing once again the superiority of algorithm `energy`.

Once model $\sigma_{\text{basic},6}$ is fitted, it also determines a horizontal axis and thus allows to compute the y-coordinates of the reference point in both imprints. Moreover, one can then compute the Euclidean distance of the two reference points in the two imprints when mapped in a single coordinate system; see Table 4.9 for the corresponding figures. To give an idea of how much coordinates necessarily vary due to distortions, we also computed the Euclidean distance between core and delta (or the corresponding barycentres for whorls, as above) in each imprint and also reported their median difference (in pixels). Undoubtedly, while the difference in the x-coordinates was not too far from this "optimum", the extraction of y-coordinates is not quite reliable – let alone the definition of both simultaneously. To get a visual impression of the size of the pixels go back to Figure 4.4 where squares with a side-length of 101 pixels

	σ_{SM}	$\sigma_{\text{basic,6+small}}$	$\sigma_{\text{basic,6+large}}$	$\sigma_{\text{basic,6+energy}}$	core-delta
orientations (in degrees)	5.8	5.8	5.8	4.7	
x-coordinates (in pixels)		23.4	21.8	15.0	
y-coordinates (in pixels)		50.9	46.3	31.9	
distances (in pixels)		69.7	60.4	41.1	8.3

Table 4.9. Median difference between orientations of axes, x- and y-coordinates, as well as median Euclidean distances of reference points extracted from loops and whorls using the models and algorithms specified; column "core-delta" gives the median difference in the distance between core and delta. See Section 4.4 for details.

fingerprint class	σ_{SM}	`small`	`large`	`energy`	core-delta
loops and whorls	0.19 (0.25)	0.16 (0.24)	0.16 (0.24)	0.14 (0.22)	0.12 (0.14)
loops	0.19 (0.24)	0.15 (0.22)	0.16 (0.23)	0.14 (0.20)	0.12 (0.13)
left loops	0.30 (0.25)	0.26 (0.22)	0.25 (0.22)	0.25 (0.22)	0.12 (0.12)
right loops	0.28 (0.23)	0.22 (0.21)	0.22 (0.20)	0.22 (0.21)	0.12 (0.14)
tented arches	0.39 (0.30)	0.34 (0.30)	0.36 (0.32)	0.30 (0.29)	0.19 (0.21)
whorls	0.22 (0.28)	0.24 (0.28)	0.21 (0.26)	0.22 (0.27)	0.15 (0.16)

Table 4.10. Average proportion (and corresponding standard deviation) of second imprints to be scanned until the one corresponding to the first imprint is found, when sorted by similarity of the angle formed by a reference axis and the specified model's or algorithm's axis, or by the distance between core and delta, respectively; as appropriate the search has been restricted to the named fingerprint class. See Section 4.4 for details.

are shown. Still, considering the difficulty of the task, one might call the results obtained by $\sigma_{\text{basic,6}}$ based on algorithm `energy` "acceptable".

Another potential use for these axes lies in database indexing: when searching for a match we could sort by the angle formed between the vertical axis and the reference axis, as described above. Naturally, this is only possible for loops and whorls but they constitute the vast majority of fingerprints. Similarly, the distance between core and delta could be used for sorting. With these "parameters" we replicated the experiment on indexing described in Section 4.3, the results of which are to be found in Table 4.10. Evidently, although the angle obtained by algorithm `energy` allows for good speed-ups, even for individual fingerprint classes, the much simpler distance of core and delta gives by far the better index, especially when taking its much lower standard deviations into account. From these figures we can also infer that the (intrinsic) locations of cores and deltas vary relatively much between the fingers in this database, which seems to constitute a rather interesting fact in itself.

Chapter 5

Discussion

Now that we have modelled orientation fields of fingerprints, proposed algorithms to fit these models, and analysed the performance of these models from various perspectives, we ought to ask ourselves the question Tukey (1977) would have asked: "How far have we come?" Let us therefore re-examine the goals we had set ourselves in Section 1.2 for the applications we had in mind.

In Chapter 2 we presented a mathematical framework, namely *quadratic differentials*, in which we not only were able to reinterpret existing models and Penrose's formula (Penrose 1969) but which allowed us to model orientation fields of fingerprints using a *minimal* set of 5 (real) parameters, each having a clear *geometric interpretation.* Out of these, 3 parameters directly modelled the Euclidean motion making the other 2 *invariant* under such transformations. Indeed, we saw in Section 4.3 that they vary relatively little between imprints of the same finger compared to their spread in the whole population. This and the models' reasonable *predictive power* further show the parameters' *robustness against partial observations* to an extent which can justly be expected from such a rigid model. Another way to look at this is via the *stability of intrinsic coordinates* as done in Section 4.4. There we saw that although algorithm `energy` allows to quite reliably extract a vertical axis, the extraction of a horizontal axis was less stable between different imprints of the same finger. Last but not least we found in Section 4.1 that the models we propose were more *accurate* than the models of Sherlock and Monro (1993) or Zhou and Gu (2004) although the latter uses much more parameters, cf. Section 3.5. We could summarise by saying that to a good extent we achieved our aims of Section 1.2.

We also explored the potential of our models for their use in different applications, see Chapter 4. The high accuracy of the models within all fingerprint classes would certainly allow to achieve high *compression* rates due to the *low dimension* of the models' parameter space; we however did not look further into that issue.

The models' usefulness for *extrapolation* on the other hand has been examined in Section 4.2 where their predictions were found to be quite accurate for arches and loops but less so for whorls, possibly due to the study design. This is an issue one might want to look at more deeply in further studies. Note however that Sherlock and Monro (1993) already observed their model's potential for prediction when they use it simply to lift the singular points in order to obtain an orientation field than can be unwrapped: classical inter- or extrapolation techniques, e.g. thin-plate splines, could then be applied to the unwrapped field. It would be interesting to see whether this method, combined with one of our newly proposed models, allows for a more accurate extrapolation as the outer field would then be modelled more accurately.

It appeared natural to employ the scaling parameters for *indexing*, see Section 4.3. In our identification scenario there, sorting by the non-conformity parameter l_r allowed for a moderate speed-up when searching through the database but for arches the gain was quite small. For the other fingerprint classes there are simpler and more efficient ways to index a database as seen in Section 4.4, namely when sorting by the distance of core(s) and delta(s).

The results in Section 4.4 also showed that *intrinsic coordinates* defined with the help of the parameters fixing the Euclidean motion will not be precise enough to directly match e.g. minutiae points in two different imprints of the same finger. Nonetheless they might be helpful in guiding this process by providing for a rough initial guess from which the correct alignment will not differ too much. Especially the relatively quick-to-extract vertical axis provided by algorithm `energy` might prove useful to this end.

Another potential application of this algorithm lies in the area of *biometric crypto-systems* recently attracting much attention: here, one aims to develop crypto-systems in which the key to unlock some remote secret is a biometric, in our case a fingerprint, cf. (Uludag et al. 2004). Because of fears about the insecurity of the transmission channel used one does not want to send the raw fingerprint to the provider of the secret. One idea is to use the minutiae points as the key. This is problematic, however, for two reasons. Firstly, the set of minutiae the secret provider stores and the set of the ones the secret seeker knows about will in general only overlap – none will be a superset of the other. Secondly, due to translations and rotations, the minutiae sets need to be aligned. The first problem can be overcome by using a so-called *fuzzy vault*, cf. (Uludag et al. 2005). To overcome the other difficulty, Uludag and Jain (2006) suggest to use *helper data* which the provider sends to the seeker so he can align his minutiae, in particular the authors suggest to use points of highest curvature as helper data. Extracting the vertical axis, as can reliably be done using algorithm `energy`, however, might be enough to enable the seeker to align his minutiae with the provider's – rendering any helper data unnecessary. This is certainly an idea whose applicability should be studied in detail.

Through the analyses carried out, and backed by further empirical results not presented here, we have found that our proposed models perform quite similar in all aspects considered. We then favoured model $\sigma_{\text{basic},6}$ although the results for model σ_{circ} differ only negligibly, while models $\sigma_{\text{basic},2}$ and $\sigma_{\text{basic},4}$ seemed slightly inferior. Regarding the methods to find the symmetry axis, however, algorithm `energy` clearly is to be preferred over the others, cf. Section 4.1.

All models and algorithms considered share a major drawback, however: they can only be applied when *all* singular points have been detected. Unfortunately, more often than not this does not happen to be the case. Although we could take the liberty to reject a fingerprint if one of its core points is missing, arguing that it lies in the central and possibly most informative area of the finger which hence should be observed well, in many applications we cannot allow ourselves this luxury if a delta goes undetected: since deltas mark the very borders of the central area, they are likely to be outside the observed fingerprint region, typically so for sweep sensors which are widely used in mobile devices such as laptops or in the forensic sciences where for obvious reasons latent fingerprints are rarely complete. It might be possible to *estimate* the location of a missing delta, though, at least accurately enough to allow for extrapolation or for the determination of a vertical axis. This seems to be a promising direction of further research which we ought to pursue.

Another open problem concerns the accuracy of our models for arches. We saw at several stages of our analyses that they performed much less satisfyingly for arches than for loops and whorls. Although this can partially be explained by the singular points determining the central field and thus providing e.g. a higher *accuracy* there, cf. Section 4.1, this seems not to be a sufficient reason for the models' parameters to be much less informative for arches, cf. Section 4.3. This appears even more estranging when considering that we actually aimed at replicating these "arches" – which we managed better than the other models but apparently not well enough. When looking back at the field created by an arch, see e.g. Figure 3.1, we observe that the curvature is the highest right in the centre of the fingerprint, the ridges in the centre look like they were forced together there. This behaviour cannot be deduced from the outer field and thus cannot be modelled by a (locally conformal) quadratic differential on $\hat{\mathbf{C}}$. A possible way to obtain better models for arches might be by looking at the bio-physical process forming them, cf. (Kücken and Newell 2004).

In conclusion, the models we have proposed and analysed provide clear improvements over prior models, as our extensive study – probably the first of its kind – has shown. Further research might however be needed to allow for their wide-spread applicability.

Bibliography

Bazen, A. M. and Gerez, S. H. (2001). Segmentation of fingerprint images, *ProRISC 2001, 12th Annual Workshop on Circuits, Systems and Signal Processing*, Veldhoven, The Netherlands, pp. 198–204.

Bazen, A. M. and Gerez, S. H. (2002). Systematic methods for the computation of the directional fields and singular points of fingerprints, *IEEE Transactions on Pattern Analysis and Machine Intelligence* **24**(7): 905–919.

Bonnevie, K. (1924). Studies on papillary patterns of human fingers, *Journal of Genetics* **15**(1): 1–111.

Brent, R. (1973). *Algorithms for Minimization without Derivatives*, Prentice-Hall, Englewood Cliffs, New Jersey.

Chen, X., Tian, J., Cheng, J. and Yang, X. (2004). Segmentation of fingerprint images using linear classifier, *EURASIP Journal on Applied Signal Processing* **2004**(4): 480–494.

Farkas, H. M. and Kra, I. (1980). *Riemann Surfaces*, Springer-Verlag, New York.

Galton, F. (1892). *Finger Prints*, Macmillan, London.

Gardiner, F. P. (1987). *Teichmüller Theory and Quadratic Differentials*, John Wiley & Sons, New York.

Grötzsch (1929). *Über konforme Abbildung unendlich vielfach zusammenhängender schlichter Bereiche mit endlich vielen Häufungsrandkomponenten*, PhD thesis, Mathematisch-naturwissenschaftliche Abteilung der Philosophischen Fakultät, Universität Leipzig. Published in *Berichte der mathematisch-physischen Klasse der Sächsischen Akademie der Wissenschaften zu Leipzig, Band 81, Heft 2*.

Gu, J. and Zhou, J. (2004). Modeling orientation fields of fingerprints with rational complex functions, *Pattern Recognition* **37**: 389–391.

Gu, J., Zhou, J. and Zhang, D. (2004). A combination model for orientation field of fingerprints, *Pattern Recognition* **37**: 543–553.

Huckemann, S., Hotz, T. and Munk, A. (2006). Global models for the orientation field of fingerprints: An approach based on quadratic differentials, submitted.

Jarre, F. and Stoer, J. (2004). *Optimierung*, Springer-Verlag, Berlin.

Jensen, G. (1975). Quadratic differentials, *in* C. Pommerenke (ed.), *Univalent Functions*, Vandenhoeck & Ruprecht, Göttingen, chapter 8.

Kerckhoff, S., Masur, H. and Smillie, J. (1986). Ergodicity of billiard flows and quadratic differentials, *Annals of Mathematics, 2nd Ser.* **124**(2): 293–311.

Kholodenko, A. L. (2000). Use of quadratic differentials for description of defects and textures in liquid crystals and 2+1 gravity, *Journal of Geometry and Physics* **33**(1-2): 59–102.

Kücken, M. and Newell, A. C. (2004). A model for fingerprint formation, *Europhysics Letters* **68**(1): 141–146.

Maio, D., Maltoni, D., Cappelli, R., Wayman, J. L. and Jain, A. K. (2002). FVC2000: Fingerprint verification competition, *IEEE Transactions on Pattern Analysis and Machine Intelligence* **24**(3): 402–412.

Maltoni, D., Maio, D., Jain, A. K. and Prabhakar, S. (2003). *Handbook of Fingerprint Recognition*, Springer, New York.

Mardia, K. V. and Jupp, P. E. (2000). *Directional Statistics*, Wiley, Chichester.

Mardia, K. V., Li, Q. and Hainsworth, T. J. (1992). On the Penrose hypothesis on fingerprint patterns, *IMA Journal of Mathematics Applied in Medicine & Biology* **9**: 289–294.

Nelder, J. A. and Mead, R. (1965). A simplex algorithm for function minimization, *Computer Journal* **7**: 308–313.

Penrose, L. S. (1969). Dermatoglyphics, *Scientific American* **221**(6): 73–84.

R Development Core Team (2006). *R: A Language and Environment for Statistical Computing*, R Foundation for Statistical Computing, Vienna, Austria. ISBN 3-900051-07-0.

Sherlock, B. G. and Monro, D. M. (1993). A model for interpreting fingerprint topology, *Pattern Recognition* **26**(7): 1047–1055.

Smith, C. A. B. (1979). Note on the forms of dermatoglyphic patterns, *Dermatoglyphics: Fifty Years Later*, Vol. 15 of *Birth Defects: Original Article Series*, The National Foundation, pp. 43–52.

Strebel, K. (1984). *Quadratic Differentials*, Springer, Berlin.

Teichmüller, O. (1940). *Extremale quasikonforme Abbildungen und quadratische Differentiale*, number 1939,22 in *Abhandlungen der Preußischen Akademie der Wissenschaften, Mathematisch-naturwissenschaftliche Klasse*, Verlag der Akademie der Wissenschaften, Berlin.

Tukey, J. W. (1977). *Exploratory Data Analysis*, Addison-Wesley Publishing Company, Reading, Massachusetts.

Uludag, U. and Jain, A. K. (2006). Securing fingerprint template: Fuzzy vault with helper data, *CVPRW '06: Proceedings of the 2006 Conference on Computer Vision and Pattern Recognition Workshop*, IEEE Computer Society, Washington, D.C., p. 163.

Uludag, U., Pankanti, S. and Jain, A. K. (2005). Fuzzy vault for fingerprints, *Proc. AVBPA 2005, 5th Internatinal Conference on Audio- and Video-Based Biometric Person Authentication*, pp. 310–319.

Uludag, U., Pankanti, S., Prabhakar, S. and Jain, A. K. (2004). Biometric cryptosystems: Issues and challenges, *IEEE Transactions on Pattern Analysis and Machine Intelligence* **92**(6): 948–960.

Verbov, J. (1970). Clinical significance and genetics of epidermal ridges – a review of dermatoglyphics, *The Journal of Investigative Dermatology* **54**(4): 261–271.

Vizcaya, P. R. and Gerhardt, L. A. (1996). A nonlinear orientation model for global description of fingerprints, *Pattern Recognition* **29**(7): 1221–1231.

Watson, C. I. and Wilson, C. L. (1992). *NIST Special Database 4: Fingerprint Database*, National Institute of Standards and Technology.

Zhou, J. and Gu, J. (2004). Modeling orientation fields of fingerprints with rational complex functions, *Pattern Recognition* **37**: 389–391.

Curriculum Vitae

Thomas Hotz (dipl. math.)

born 25 February 1978, Bruchsal
married, German

September 1984 – June 1997	Schooling *Abitur* at *Leibniz-Gymnasium Östringen* *Scheffelpreis* (school award for German)
July 1997 – April 1998	Military Service
April 1998 – September 2002	Study of Mathematics and Computer Science (minor) *Faculty of Mathematics, University of Heidelberg* diploma thesis: *On the Consistency of the Minimum Description Length Criterion* supervised by *Prof. Dr. Rainer Dahlhaus*
January 1999 – March 2002	Research Assistant (unexamined) *Faculty of Mathematics, University of Heidelberg*
October 2002 – September 2003	Research Associate in Medical Statistics *Trent Institute for Health Services Research* *Department of Epidemiology and Public Health* and *Department of Medicine, University of Leicester, U.K.*
October 2003 – October 2004	Associate Statistician *United Nations Statistics Division, New York, U.S.A.*
April 2006 – September 2006	Research Assistant (examined) *Institute for Mathematical Stochastics* *University of Göttingen*
since November 2004	Ph.D. Studies in Mathematics *Faculty of Mathematics, University of Göttingen* supervised by *Prof. Dr. Axel Munk* funded member of the *DFG Graduate Program 1023*